Mucin-type *O*-glycans regulate proteoglycan stability and chondrocyte maturation

Xiaolin Dong[1,2], Sydney Bedillion[1,2], Kaleigh E. Gosnell [2], Peng Zhao[1], Amrita Basu[1], Kavya Suryadevara[2], Digantkumar Chapla[1], Lance Wells[1,2], Ryan J. Weiss[1,2]*

[1]Complex Carbohydrate Research Center, University of Georgia, Athens, Georgia 30602, United States

[2]Department of Biochemistry and Molecular Biology, University of Georgia, Athens, Georgia 30602, United States

Running Title: ***O*-GalNAc glycans regulate proteoglycan stability and chondrogenesis**

*To whom correspondence should be sent:

Ryan J. Weiss, Ph.D.

Complex Carbohydrate Research Center

University of Georgia

315 Riverbend Road

Athens, GA 30602

E-mail: ryan.weiss@uga.edu

Phone: 706/542-6445 FAX: 706/542-4412

Keywords: glycosaminoglycans, heparan sulfate, proteoglycans, *O*-GalNAc, *O*-glycosylation, chondrocytes, chondrogenesis

Abstract

O-glycosylation is a ubiquitous post-translational modification essential for protein stability, cell signaling, and tissue organization, yet how distinct *O*-glycan subclasses coordinate tissue development remains unclear. Here, we identify functional crosstalk between extended mucin-type *O*-glycans and heparan sulfate proteoglycans (HSPGs). Genetic ablation of β-1,3-galactosyltransferase 1 (C1GALT1) or its chaperone COSMC in human chondrocytes reduced cell surface HSPGs and fibroblast growth factor (FGF) binding, leading to impaired MAPK/ERK signaling, which was recapitulated in hypomorphic *COSMC-CDG* patient cells. Transcriptomic and secretome analyses revealed selective loss of proteoglycan expression and broader extracellular matrix remodeling in COSMC- and C1GALT1-deficient cells. Mechanistically, truncation of *O*-GalNAc glycans reduced Syndecan-1 levels at the cell surface via enhancing its lysosome-dependent degradation and diminished CD44v3-mediated FGF1 binding. Functionally, loss of complex *O*-GalNAc glycans disrupted chondrogenesis of growth plate-like chondroprogenitors. Overall, these findings reveal previously unrecognized roles for mucin-type *O*-glycans in maintaining proteoglycan stability and function, highlighting cross-regulatory mechanisms of glycosylation crucial for normal development that likely contribute to the pathophysiology of glycosylation-related disorders.

39 **Introduction**

40 Glycosylation confers structural complexity to the proteome, directing protein folding,
41 trafficking, and stability while orchestrating processes essential for tissue development and
42 homeostasis[1, 2]. Increasing evidence indicates that distinct glycosylation pathways are
43 interconnected, with one type of glycan influencing the efficiency, content, and spatial
44 organization of others[3]. This coordination could arise through shared nucleotide-sugar precursors
45 and/or diverse forms of glycosylation on the same protein, which together can influence protein
46 assembly, trafficking, and function. Such dynamic cross-regulation among glycans is increasingly
47 recognized as a key determinant of cell surface organization, receptor recognition, and cellular
48 function[4, 5], yet the molecular mechanisms governing this interplay remain poorly understood.

49 Among the diverse forms of glycosylation, *O*-glycans represent the most common covalent
50 modifications of serine and threonine residues of mammalian glycoproteins. Two major
51 subclasses of *O*-glycans, mucin type *O*-GalNAc glycans and glycosaminoglycans (GAGs), exhibit
52 distinct but complementary roles in tuning protein function and extracellular matrix (ECM)
53 assembly[5]. *O*-GalNAc glycans are among the most abundant and diverse types of *O*-
54 glycosylation. *O*-GalNAcylation is initiated in the Golgi apparatus by polypeptide GalNAc-
55 transferases (ppGalNAc-Ts) enzymes. These enzymes attach *N*-acetylgalactosamine (GalNAc)
56 to serine or threonine residues, forming the Tn antigen. Next, the core 1 β1,3-
57 galactosyltransferase (C1GALT1), along with its obligate molecular chaperone, COSMC
58 (*C1GALT1C1*, an X-linked gene on Xq24), adds galactose to form the T antigen (core 1 *O*-glycan).
59 This core 1 structure serves as the required platform for the generation of a large assortment of
60 elaborated core structures to produce the full array of mature *O*-glycans[6]. Mature mucin-type O-
61 glycans regulate protein folding, secretion, protein-glycan binding, and cell-cell interactions,
62 whereas their truncation is a hallmark of several diseases, including cancer and rare genetic

63 disorders[7, 8]. Importantly, *O*-GalNAc glycans can also act as Golgi export signals, which influences
64 the secretion, stability, and localization of glycoproteins and tissue organization[9].

65 Glycosaminoglycans (GAG) are long, linear polysaccharides consisting of repeating
66 glucosamine (GlcN) and glucuronic/iduronic acid (GlcA/IdoA) subunits that are variably sulfated
67 and *O*-linked to serine residues of core proteins, known as proteoglycans (PGs)[10, 11]. Two principal
68 GAG subclasses, heparan sulfate (HS) and chondroitin/dermatan sulfate (CS/DS), are essential
69 components of the cell surface and extracellular matrix (ECM) and are ubiquitously expressed in
70 animal tissues. HS and CS/DS proteoglycans collectively regulate cell signaling and homeostasis
71 by binding growth factors, integrins, and ECM proteins[12]. Their structural diversity in chain length
72 and sulfation pattern fine-tunes these interactions, controlling cell adhesion, migration, and tissue
73 morphogenesis[10]. In skeletal tissues, for example, proteoglycans form complexes with collagen
74 and hyaluronan that provide structural integrity and guide cartilage and bone development[13].

75 Defects in *O*-GalNAc or GAG biosynthesis underlie a subset of rare genetic disorders,
76 known as congenital disorders of glycosylation (CDGs), which manifest with pleiotropic effects on
77 cell function across tissues[14, 15]. Many CDG disorders exhibit pleiotropic overlapping clinical
78 features, including developmental disabilities, multi-organ involvement, short stature, and skeletal
79 abnormalities[16]. For example, a recent study revealed that *COSMC*-CDG patients, caused by
80 inherited mutations in *COSMC/C1GALT1C1 (*A20D-COSMC*)*, frequently exhibit skeletal defects
81 and short stature in addition to other systemic issues[15]. Similarly, *EXT1/EXT2*-CDG, commonly
82 known as Multiple Hereditary Exostoses (MHE), results from heterozygous mutations in *EXT1* or
83 *EXT2*, which encode glycosyltransferases essential for heparan sulfate elongation, leading to the
84 formation of bony outgrowths that cause chronic pain and can interfere with normal bone
85 development[17]. Interestingly, a recent study reported that mice with chondrocyte-specific
86 transgenic expression of *Galnt3*, a polypeptide GalNAc transferase encoding gene, exhibit
87 enhanced Tn antigen levels at the growth plate, which coincided with decreased GAG levels,
88 dwarfism, reduced chondrocyte maturation, and skeletal dysplasia[18]. These findings point to

89 functional cross-regulation between *O*-GalNAc glycosylation and proteoglycan assembly.
90 Additionally, the convergence of skeletal defects across distinct CDGs implies a shared
91 requirement for coordinated *O*-glycan and proteoglycan regulation during development.

92 Although the majority of membrane-bound and secreted proteoglycans also carry *O*-
93 GalNAc glycans[19], direct mechanistic evidence linking *O*-GalNAc glycosylation to proteoglycan
94 stability and function remains lacking. Here, we tested the hypothesis that mucin-type O-glycans
95 regulate proteoglycan trafficking and cell surface presentation. Using CRISPR/Cas9-mediated
96 knockout of *COSMC* or *C1GALT1*, respectively, in human and murine chondrocytes, we
97 demonstrate that truncation of mucin-type *O*-GalNAc glycans destabilizes cell-surface
98 proteoglycans and alters ECM composition. Transcriptomic and secretomic profiling indicated
99 global remodeling of proteoglycan biosynthesis and secretion in COSMC/C1GALT1 deficient
100 cells, while in vitro differentiation assays using a cell-based model of the growth plate revealed
101 impaired chondrogenic maturation. Together, these findings uncover a fundamental cross-
102 regulatory mechanism linking mucin-type *O*-glycosylation and proteoglycan function that reveals
103 new insights into *O*-glycan functions in development and glycosylation-related disorders.

104 **Results**

105 **Global truncation of *O*-GalNAc glycans reduces HSPGs and impairs HS-dependent growth**
106 **factor binding and signaling**

107 To assess whether mucin-type *O*-GalNAc glycosylation influences proteoglycan
108 biosynthesis and cell surface presentation, we genetically disrupted the core 1 *O*-glycan
109 biosynthetic pathway in human chondrocytes. For our studies, we utilized immortalized TC28a2
110 human chondrocytes, which highly express cell-surface proteoglycans and serve as a tractable
111 in vitro model to study the cross regulation of *O*-GalNAc glycans and proteoglycans in cartilage[20,
112 21]. With over 20 known ppGalNAc-Ts (GALNTs), genetic redundancy makes disrupting *O*-GalNAc
113 initiation via a single gene knockout challenging[22, 23]. In addition, studies have shown that loss of

114 individual GALNTs often leads to substrate-specific effects rather than global abolition of *O*-
115 GalNAcylation[24]. Instead, we utilized CRISPR/Cas9 to globally truncate *O*-GalNAc glycans
116 through genetic ablation of β1,3-galactosyltransferase (*C1GALT1*) or its chaperone, COSMC
117 (*C1GALT1C1*), which coordinate to add galactose (Gal) to GalNAc to generate the T antigen at
118 serine/threonine residues of the core protein and thus eliminates the production of both Core 1
119 and Core 2 extended *O*-GalNAc glycans[6] (Fig. 1A). Successful gene disruption was confirmed by
120 Western blotting and Sanger sequencing (Fig. 1B-C, Suppl. Fig. 1A-B). Flow cytometry following
121 pre-treatment with sialidase demonstrated robust accumulation of the Tn antigen in both knockout
122 lines, detected by VVA lectin and anti-Tn antibody cell surface staining, (Fig. 1D; Suppl. Fig. 1C),
123 accompanied by the expected corresponding loss of the Core 1 T antigen detected by PNA lectin
124 binding (Fig. 1E).

125 After confirming truncation of extended *O*-GalNAc glycans, we purified cell surface HS
126 and CS/DS polysaccharides from wild-type, *COSMC*$^{-/-}$, and *C1GALT1*$^{-/-}$ cells via anion exchange
127 chromatography and analyzed their disaccharide composition using liquid chromatography
128 coupled to mass spectrometry (LC-MS), using previously reported methods (Suppl. Fig 1D)[25, 26].
129 Interestingly, these analyses revealed a reduction in total HS levels in both *COSMC*$^{-/-}$ and
130 *C1GALT1*$^{-/-}$ knockout cells with no significant change in CS/DS content (Fig. 1F-G). HS
131 disaccharide composition remained largely unchanged, with a slight reduction in 6-*O* sulfated
132 disaccharides in the *COSMC*$^{-/-}$ knockout line (Suppl. Fig 1E-G), while CS/DS disaccharides were
133 largely unchanged in both knockout lines, with a slight decrease in 6-O sulfation in *C1GALT1*$^{-/-}$
134 cells (Suppl. Fig. 1H-I). To clarify these findings, we conducted flow cytometry using proteoglycan-
135 specific antibodies, including 3G10, which recognizes HS neoepitopes on proteoglycans
136 produced upon heparinase digestion[27], and 2B6, which detects CS neoepitopes after
137 chondroitinase ABC digestion[28] (Fig. 1H). Flow cytometry analysis revealed a ~80% reduction in
138 3G10 binding with no significant changes in 2B6 binding (Fig. 1I-J), indicating that the observed
139 decreased HS levels were due to a reduction in HSPGs and/or HS-modified sites at the cell

140 surface. Overall, these findings reveal that truncation of *O*-GalNAc glycans results in a selective
141 reduction in HSPG presentation at the cell surface in human chondrocytes.

142 HSPGs are known to function as ternary receptors for fibroblast growth factors (FGFs)
143 and their fibroblast growth factor receptors (FGFRs), thus aiding in receptor-mediated activation
144 of downstream signaling pathways, including MAPK, relevant for musculoskeletal development
145 (Fig. 2A)[29, 30]. Given that we observed a selective decrease in cell surface HS in *COSMC*$^{-/-}$ and
146 *C1GALT1*$^{-/-}$ cells, we hypothesized that truncation of *O*-GalNAc glycans would impair HS-
147 dependent FGF binding and downstream MAPK signaling. Flow cytometry analysis revealed a
148 significant decrease in cell surface binding of two well-characterized HS-binding proteins,
149 fibroblast growth factor 1 (FGF1) and fibroblast growth factor 2 (FGF2)[12, 31], in *COSMC*$^{-/-}$ and
150 C*1GALT1*$^{-/-}$ knockout cells (Fig. 2B-C). We independently confirmed these observed FGF binding
151 defects in additional *COSMC*$^{-/-}$ and *C1GALT1*$^{-/-}$ knockout clonal lines (*COSMC*^{c6}, *C1GALT1*^{t2}),
152 which also exhibited decreased 3G10 binding and increased Tn antigen levels (Suppl. Fig. 2). To
153 examine whether reduced growth factor binding was driven by alterations in FGF receptor
154 (FGFR) expression, we measured FGFR1 cell surface levels, which is highly expressed in
155 TC28a2 cells, via flow cytometry using an FGFR1-specific antibody. This analysis revealed
156 minimal differences in FGFR1 levels between wild-type and knockout lines (Fig. 2D), suggesting
157 an HS-dependent reduction in FGF binding at the cell surface. Consistent with reduced cellular
158 HS levels and FGF binding, FGF2-induced ERK1/2 phosphorylation was also significantly
159 reduced in *COSMC*$^{-/-}$ and *C1GALT1*$^{-/-}$ knockout cells compared to wild-type controls (Fig. 2E-F).

160 To rule out off-target effects driving the observed phenotypes, full-length human C1GALT1
161 cDNA was reintroduced in *C1GALT1*$^{-/-}$ knockout cells (Fig. 2G), which restored cell surface
162 binding of FGF2 (Fig. 2H), thus linking truncation of *O*-GalNAc glycans to a decrease in cell
163 surface HS content and function. Importantly, we also validated our findings in primary fibroblasts
164 isolated from a male *COSMC-CDG* patient with the hemizygous variant c.59C>A (p.Ala20Asp) in

165 *C1GALT1C1* (A20D-COSMC). These cells were reported to exhibit similar defects in *O*-glycan
166 extension and accumulate Tn antigen[15], which we confirmed by VVA binding (Fig. 2I). Intriguingly,
167 the *COSMC-CDG* patient-derived cells also exhibited a reduction in 3G10, FGF1, and FGF2
168 binding, albeit with more subtle defects compared to TC28a2 knockout lines, which we attributed
169 to low residual T-synthase enzyme activity, as previously reported[15]. Collectively, these results
170 establish *O*-GalNAcylation as a key regulator of HS-mediated growth factor binding and
171 signaling, with critical implications for cell growth and signaling.

172 **Mucin-type *O*-GalNAc glycans regulate proteoglycan expression and secretion**

173 We next aimed to understand the underlying molecular mechanisms leading to reduced
174 proteoglycan cell surface presentation in COSMC/C1GALT1 deficient cells. First, we performed
175 RNA sequencing on wild-type, *COSMC*$^{-/-}$, and *C1GALT1*$^{-/-}$ knockout cells to compare their
176 transcriptome profiles. A heat map of global differential expression changes revealed distinct
177 hierarchical clustering for *COSMC*$^{-/-}$ and *C1GALT1*$^{-/-}$ knockout cells compared to wild-type, with
178 128 overlapping genes significantly downregulated and 219 genes upregulated (Fold change ≥ 2,
179 FDR $p \leq 0.01$) in both knockout cells (Fig. 3A-B, Suppl. Fig. 3A-B). Gene ontology analysis of the
180 shared differentially expressed gene sets revealed downregulation of pathways related to
181 *extracellular matrix organization*, *retrograde signaling*, and *syndecan interactions* as well as
182 upregulation of pathways related to the *inflammatory response*, *tube morphogenesis*, and
183 *transcriptional misregulation*, consistent with broad effects of *O*-glycan truncation on transcription
184 and associated cellular processes (Fig. 3C-D). When we compared specific expression changes
185 for all GAG-related enzymes and proteoglycans, we found that the largest subset of differentially
186 expressed GAG genes (FDR $p \leq 0.01$) encoded proteoglycans, including downregulation of
187 several HSPGs (*SDC2, HSPG2, GPC1, GPC6, COL18A1*) and upregulation of "part-time"
188 proteoglycans, *CD44* and *ESM1*[32], among others (Fig. 3E). In addition, expression of a subset of
189 GAG biosynthetic genes was altered in both knockout lines, including downregulation of the

190 secreted HS endosulfatases, *SULF1/SULF2,* and upregulation of CS biosynthetic enzymes,
191 *CHST11* and *CSGALNACT1* (Fig. 3E). The top differentially expressed hits in this set (*SULF1,*
192 *SULF2, SDC2, ESM1*) were also confirmed in the additional *COSMC*^{c6} and *C1GALT1*^{t2} knockout
193 lines via quantitative PCR (Suppl. Fig. 3C). Among the top hits, we focused on one of the most
194 significantly downregulated genes, Syndecan-2 (*SDC2*), which encodes a key transmembrane
195 HSPG that is a known co-receptor for FGFs and plays roles in tissue development and repair[33].
196 We orthogonally confirmed a decrease in cell surface SDC2 levels in both knockout lines via flow
197 cytometry using an anti-SDC2 antibody (Fig. 3F), consistent with the observed reduction in mRNA
198 levels (Fig. 3E). Notably, we assessed cell surface levels of a related syndecan protein,
199 Syndecan-1 (SDC1), which exhibited a slight increase in mRNA levels with a surprising significant
200 decrease in cell surface levels in *COSMC*$^{-/-}$ and *C1GALT1*$^{-/-}$ knockout cells (Fig. 3G). This
201 discrepancy between *SDC1* transcript level changes and reduced protein abundance at the cell
202 surface suggested that SDC1 protein may be regulated post-translationally in cells lacking
203 complex *O*-GalNAc glycans, possibly via enhanced shedding and/or reduced cell surface
204 trafficking.

205 Prior work has highlighted the importance of *O*-GalNAc glycosylation for the trafficking
206 and secretion of extracellular proteins, which directly influences ECM composition and impacts
207 cell adhesion, growth and organogenesis[34, 35, 36]. Additionally, glycomics-based studies using the
208 SimpleCell technology previously identified *O*-GalNAc modified sites on multiple proteoglycans,
209 including SDC1[23, 37]. To identify the repertoire of *O*-GalNAc modified proteoglycans in TC28a2
210 chondrocytes, we adapted our selective exoenzymatic labeling (SEEL) method[38] to detect Tn
211 antigen modified sites in the *COSMC/C1GALT1* knockout lines using CMP-sialic acid-biotin
212 (CMP-sia-biotin) and recombinant ST6GALNAC1 (Suppl. Fig. 4A), which adds a sialic acid to *O*-
213 GalNAc of the Tn antigen[39]. Cells were incubated with sialidase and labeled with ST6GALNAC1
214 in the presence of CMP-sia-biotin followed by streptavidin enrichment (Suppl. Fig. 4B). Both
215 knockout lines gave substantial labeling in the presence of CMP-sia-biotin by western blotting

216 with streptavidin (Suppl. Fig. 4C), and LC-MS/MS proteomic analysis confirmed enrichment of
217 multiple known *O*-glycosylated cell surface/ECM proteins (e.g., CD44, LDLR, FN1, DAG1)
218 including several HSPGs (SDC1, SDC2, SDC4, GPC1, GPC6) (Suppl. Fig. 4D), most of which
219 have been previously identified as *O*-GalNAc modified in other cells and/or tissues in recent
220 studies[23, 40, 41].

221 Next, we probed whether targeting *COSMC* or *C1GALT1* alters the secreted proteome in
222 TC28a2 chondrocytes. We collected conditioned media from cultured wild-type, *COSMC*$^{-/-}$, and
223 *C1GALT1*$^{-/-}$ cells, respectively, and profiled the secreted proteome by LC-MS/MS by adapting
224 published methods (Fig. 4A) [42, 43]. This method revealed that truncation of *O*-GalNAc glycans led
225 to remodeling of the secreted proteome, with a total of 62 proteins significantly altered in
226 abundance in *COSMC*$^{-/-}$ cells and 92 proteins in *C1GALT1*$^{-/-}$ cells, respectively. Notably, we
227 identified 48 differentially secreted proteins shared between both knockout lines (Fig. 4B).
228 Consistent with previous studies[44, 45], we observed increased secretion of the *O*-glycoprotein LDL
229 receptor (LDLR) in both knockout lines (Fig. 4C-D), with no significant alterations in *LDLR* mRNA
230 expression. The top protein depleted in both knockout lines, the matrix metalloprotease MMP1,
231 exhibited a concurrent decrease in mRNA expression, while additional factors associated with
232 ECM remodeling (MMP9) and chemotaxis (CXCL1, CXCL8) were significantly decreased in the
233 secretome from *COSMC*$^{-/-}$ and *C1GALT1*$^{-/-}$ cells despite a significant increase in mRNA levels.
234 Several ECM proteoglycans (BGN, HSPG2, COL18A1) showed a reduction at both the
235 transcriptome and secretome levels, while others (AGRN, SRGN) exhibited increased abundance
236 in conditioned media with no corresponding mRNA expression changes. We detected only a
237 single cell surface HSPG (SDC4) in the *C1GALT1*$^{-/-}$ secretome, suggesting that shedding of cell
238 surface proteoglycans was minimally impacted in the *COSMC/C1GALT1* knockout cells.

239 **Truncation of *O*-GalNAc glycans reduces cell surface SDC1 via enhanced lysosomal**
240 **degradation**

241 Among the proteoglycans examined, SDC1 displayed an unexpected discordance
242 between transcript and cell surface abundance. While RNA-seq and secretome proteomics
243 showed no major changes in SDC1 mRNA or shedding, flow cytometry analyses revealed a
244 pronounced decrease in SDC1 cell surface levels (Fig. 3E-F). This discrepancy suggested that
245 truncation of complex *O*-GalNAc glycans might influence SDC1 stability and/or turnover rather
246 than its transcription or shedding. To investigate whether SDC1 trafficking to the cell surface was
247 impaired in COSMC/C1GALT1 mutants, we lifted wild-type or knockout cells with trypsin,
248 respectively, re-plated them, then monitored recovery of SDC1 at the cell surface over time via
249 flow cytometry. SDC1 protein levels were restored to the respective undigested cells after 24
250 hours at comparable initial rates in both wild-type and knockout cells, despite decreased steady-
251 state SDC1 levels in the COSMC/C1GALT1 deficient lines, indicating that SDC1 trafficking was
252 largely preserved (Fig. 5A-B). Given that SDC1 delivery to the cell surface appeared intact, we
253 next tested whether diminished SDC1 levels in COSMC/C1GALT1 knockout cells resulted from
254 decreased stability and/or increased degradation consequent to the loss of complex *O*-GalNAc
255 glycans. Since SDC1 degradation primarily occurs through endocytosis and lysosomal
256 degradation[46], we tested whether inhibition of lysosomal activity would restore SDC1 levels in
257 COSMC/C1GALT1 knockout cells. Cells were treated with bafilomycin A1, a V-ATPase inhibitor
258 that impedes lysosomal degradation[47], and cell surface and total SDC1 levels were monitored via
259 flow cytometry. After a 16-hour incubation with bafilomycin A1, we observed a significant increase
260 in both total and cell surface SDC1 levels in *COSMC*$^{-/-}$ and *C1GALT1*$^{-/-}$ cells versus vehicle-treated
261 cells (Fig. 5C-E). Confocal imaging corroborated these findings, confirming a complete rescue of
262 SDC1 levels in *COSMC*$^{-/-}$ and *C1GALT1*$^{-/-}$ cells treated with bafilomycin (Suppl. Fig. 5A-D).
263 Together, these results indicate that loss of complex O-GalNAc glycans destabilizes SDC1 at the
264 cell surface, promoting its endolysosomal-dependent degradation.

265 **Mucin-type *O*-glycans stabilize cell surface CD44 and regulate CD44v3-FGF1 binding**

266 CD44 is a highly *O*-glycosylated protein[23, 48] and is a major cell surface receptor on
267 chondrocytes that mediates cell adhesion to the extracellular matrix and participates in matrix
268 organization and turnover[49, 50]. Notably, CD44 can serve as a "part-time" proteoglycan, where a
269 specific CD44 variant, CD44v3, is modified by a single HS chain that can function as a key co-
270 receptor for growth factors, including FGF1[51] (Fig. 6A). Thus, we investigated whether full length
271 CD44 and/or CD44v3 expression was altered in *COSMC/C1GALT1* knockout cells and whether
272 this may contribute to defects in HSPG presentation and growth factor binding. Despite increased
273 *CD44* transcript levels in both knockout lines (Fig. 3E), immunoblotting and flow cytometry
274 experiments revealed a marked decrease in full-length CD44 protein levels and a lower apparent
275 molecular weight, consistent with loss of complex *O*-glycans (Fig. 6B-C). These results were
276 reproducible in independent *COSMC* and *C1GALT1* knockout clones (Suppl. Fig. 6).
277 Reintroduction of human C1GALT1 into *C1GALT1*$^{-/-}$ cells restored cell surface CD44 levels,
278 confirming a direct link between *O*-glycan truncation and CD44 presentation (Fig. 6D).
279 Mechanistically, we also found that cell surface CD44 on COSMC/C1GALT1 deficient cells
280 exhibited increased susceptibility to trypsin-mediated cleavage, with reduced steady-state levels
281 24 hours post-trypsinization (Suppl. Fig. 6B), indicating that loss of *O*-GalNAc glycans exposes
282 the CD44 ectodomain to enhanced proteolytic turnover at the cell surface. Finally, we also
283 confirmed cell surface expression of CD44v3 in TC28a2 cells using a CD44v3-specific antibody,
284 which showed a marked reduction in both knockout lines (Fig. 6E). To directly assess whether
285 decreased cell surface CD44v3 affects HS-dependent FGF binding, we generated a *CD44*$^{-/-}$
286 knockout line in TC28a2 chondrocytes, validated by Western blot and Sanger sequencing (Fig.
287 6F, Supplementary Fig. 6C). Both full length CD44 and CD44v3 were depleted in these cells,
288 respectively (Fig. 6F-G). Importantly, *CD44*$^{-/-}$ cells exhibited reduced 3G10 and FGF1/FGF2
289 binding at the cell surface (Fig. 5H-J), closely phenocopying *COSMC*$^{-/-}$ and *C1GALT1*$^{-/-}$ cell lines
290 and highlighting the important role of CD44 as a cell surface receptor in chondrocytes.

291 **Ablation of *Cosmc/C1galt1* impairs chondrogenic maturation and cartilage matrix**
292 **formation in growth plate-like chondroprogenitors**

293 Given our findings that truncation of *O*-GalNAc glycans destabilizes cell surface
294 proteoglycans and impairs cell signaling, we next investigated whether mucin-type *O*-
295 glycosylation influences chondrocyte differentiation. To test this, we employed CRISPR/Cas9 to
296 ablate *Cosmc* or *C1galt1* in murine growth plate-like chondroprogenitors (GPLCs), an established
297 in vitro model of the epiphyseal growth plate[52, 53]. Clonal knockout lines were validated by Sanger
298 sequencing and VVA/PNA lectin binding (Fig. 7A-B, Suppl. Fig. 7A). *Cosmc*$^{-/-}$ and *C1galt1*$^{-/-}$ cells
299 exhibited significantly reduced 3G10 staining and diminished cell surface binding of FGF1 and
300 FGF2 (Fig. 7C-E), accompanied by reduced CD44 (Fig. 7F), mirroring our results in human
301 TC28a2 chondrocytes. When cultured in high-density micromass and stimulated with insulin-
302 transferrin-selenium (ITS) to promote chondrogenic maturation[54], *Cosmc*$^{-/-}$ and *C1galt1*$^{-/-}$ cells
303 exhibited significantly reduced Alcian blue staining at Day 7 (Fig. 7G-H), indicating impaired
304 glycosaminoglycan-rich cartilage matrix deposition[55]. Furthermore, expression of key matrix
305 genes, *Acan* and *Col2a1*[56], was reduced (Fig. 7I-J), while *Sox9* expression remained unchanged
306 (Fig. 7K), suggesting that lineage commitment was preserved but downstream matrix elaboration
307 and maturation were impaired. Overall, these data suggest that truncation of *O*-GalNAc glycans
308 disrupts proteoglycan stability and HS-dependent signaling necessary for chondrogenic
309 maturation.

310 **Discussion**

311 In this study, we report that complex mucin-type *O*-glycosylation regulates proteoglycan
312 expression, stability, and function. Through CRISPR-mediated genetic ablation of
313 *COSMC*/*C1GALT1*, transcriptomic and proteomic profiling, and functional analyses, we show
314 that loss of extended *O*-GalNAc glycans impairs cell surface presentation of SDC1 and CD44,

315 limits heparan sulfate presentation, and attenuates growth factor-dependent signaling and
316 chondrogenesis. These findings uncover a mechanistic link between *O*-GalNAc glycan
317 maturation and proteoglycan biology, revealing that crosstalk between glycosylation pathways
318 contributes to proper extracellular matrix organization and cartilage differentiation.

319 Our studies intriguingly identified a selective reduction in cell surface HSPG presentation
320 in chondrocytes following loss of extended core 1 *O*-glycans, with seemingly minimal effects on
321 HS and CS/DS composition (Fig. 1, Suppl. Fig. 1). The specificity of this effect would suggest
322 that *O*-GalNAcylation preferentially influences the biosynthesis or stability of HSPG core proteins
323 rather than global glycosaminoglycan chain synthesis. The ~6-fold higher prevalence of HS
324 chains versus CS/DS at the cell surface of TC28a2 chondrocytes (Fig. 1F-G) likely drives the
325 observed impact of truncated *O*-GalNAc glycans on HSPG presentation. There are likely
326 differential effects on proteoglycan presentation in different cell types and tissues, largely
327 dependent on gene expression profile and site-specific glycosylation of proteoglycans. Notably,
328 our work also highlighted differential effects on proteoglycan secretion in *COSMC/C1GALT1*
329 knockout cells (Fig. 4), with altered abundance of certain ECM HSPGs (HSPG2, COL18A1,
330 AGRN, SRGN) and CSPGs (BGN, VCAN), suggesting that extended *O*-GalNAc glycans likely
331 regulate both proteoglycan secretion and their cell surface stability. The observed impact on
332 shedding and secretion of ECM proteins is supported by previous studies implicating mucin-type
333 *O*-glycans as regulators of protein trafficking and secretion[57, 58, 59, 60]. Our results extend this
334 paradigm by showing that *O*-GalNAc truncation impairs the stability and persistence of HSPGs,
335 including SDC1 and the "part-time" proteoglycan CD44v3, thereby altering the abundance and
336 organization of HS chains at the cell surface in chondrocytes.

337 A previous study reported that chondrocyte-specific overexpression of *Galnt3*, a
338 ppGalNAc-transferase, increased Tn-antigen levels and reduced GAG production in mice and
339 resulted in defects in chondrocyte organization, hypertrophy, and skeletal development[18],
340 suggesting that *O*-GalNAc initiation influences proteoglycan synthesis and function. It is possible

341 that overexpression and/or knockout of *Galnt3* leads to competition of *O*-glycan initiation at serine
342 residues within the proteoglycan core, where xylosyltransferases (XYLT1/XYLT2) can add xylose
343 to initiate GAG assembly (Fig. 1H). The site-specific regulation of diverse *O*-glycan modifications
344 on their respective protein attachment sites is still largely unknown, with evidence of amino acid
345 sequence[61] and/or substrate specificity of the enzymes[24] likely contributing to *O*-glycan initiation.
346 Enrichment of VVA lectin staining and Tn antigen presentation reported in *Galnt3* transgenic
347 mice[18] mimics the observed phenotypes in *COSMC/C1GALT1* deficient chondrocytes generated
348 in the current study. Together, these findings suggest that truncation of *O*-GalNAc glycans
349 contributes to reduced proteoglycan expression and destabilization of cell surface PGs, potentially
350 leading to skeletal defects at the growth plate. Future studies will investigate how conditional
351 ablation of C1GALT1/COSMC at the growth plate in animal models impacts skeletal development.
352 The results presented in the current study reveal distinct mechanisms by which loss of
353 complex *O*-GalNAc glycans alters proteoglycan dynamics, including transcriptional
354 downregulation of genes encoding proteoglycans (Fig. 3) and destabilization of HSPGs at the
355 cell surface. Specifically, despite upregulation of *SDC1* and *CD44* mRNA expression in
356 *COSMC/C1GALT1* knockout cells, we found that both these proteins, which are both highly *O*-
357 GalNAcylated[23, 37], required complex mucin-type *O*-glycosylation for proper cell surface
358 presentation on chondrocytes. Reduced SDC1 protein levels were caused by enhanced
359 lysosomal degradation (Fig. 5) rather than decreased synthesis or enhanced shedding/secretion
360 (Figs. 3-4), and decreased CD44 levels were likely caused by increased susceptibility to
361 proteolysis upon loss of extended *O*-GalNAc glycans (Suppl. Fig. 6), consistent with prior
362 studies[48]. In addition, loss of a specific HS-modified CD44 variant, CD44v3, contributed to
363 reduced HS-protein interactions at the cell surface (Fig. 6). Overall, these findings shed light on
364 the multi-functional roles of mucin-type *O*-glycans in regulation of proteoglycan stability and
365 function.

366 Clinically, CDG disorders often present with skeletal abnormalities, including *COSMC-*
367 *CDG*[15] and MHE[17]. Our in vitro chondrogenesis model of the growth plate revealed that truncation
368 of *O*-GalNAcylation led to decreased chondrogenic differentiation and reduced expression of key
369 cartilage matrix genes (Fig. 7). Since HSPGs are crucial for bone development, genetic defects
370 in mucin-type *O*-glycan assembly would negatively impact HSPG presentation and function, thus
371 contributing to skeletal and cartilage defects found across CDG disorders. Interestingly, *COSMC-*
372 *CDG* patient-derived fibroblasts, which harbor a hypomorphic mutation in *COSMC* and exhibit
373 reduced T-synthase activity[15], also showed reduced cell surface HSPGs and FGF binding (Fig.
374 2I), suggesting other cell types may also be similarly impacted. Therapeutically, restoring HSPG
375 function or supplementation of functional HSPGs may represent promising strategies to mitigate
376 selected clinical manifestations associated with impaired glycosylation in patients. Beyond CDGs,
377 truncated *O*-GalNAc glycans are a hallmark found in multiple cancers, where the Tn antigen
378 regulates tumor cell proliferation, differentiation, and other oncogenic features[8, 62, 63]. Cancer
379 progression also depends on proteoglycan function[64]; thus, regulation of mucin-type *O*-
380 glycosylation may also alter proteoglycan abundance and composition in tumor cells, potentially
381 aiding tumor invasion and metastasis.

382 Collectively, our results support a model in which extended *O*-GalNAc glycans stabilize
383 proteoglycan core proteins, preserve HS chain presentation, and maintain FGF-FGFR signaling
384 essential for cartilage development (Fig. 8). More broadly, our findings suggest that glycan cross-
385 regulation plays a crucial role in cellular function, development, and disease progression. These
386 findings underscore the interplay between *O*-GalNAcylation and proteoglycan structure and
387 function and illustrate the role of diverse glycosylation pathways in shaping the cell surface
388 proteome. Future studies will define how specific *O*-GalNAc sites on proteoglycan core proteins
389 regulate their folding, export, and stability, and whether targeted manipulation of *O*-glycan
390 processing can restore proteoglycan function in disease contexts. Given the emerging evidence
391 of glycan interdependence across cell types and tissues, elucidating these mechanisms will

392 deepen our understanding of glycosylation crosstalk and may identify new therapeutic
393 opportunities for glycosylation disorders.

394 **Materials and methods**

395 **Cell culture**

396 TC28a2 (Sigma-Aldrich #SCC042) and HEK293T cells (ATCC CRL-3216) were cultured in
397 DMEM (Gibco) with 10% (v/v) FBS (Gibco) and 1% (v/v) penicillin/streptomycin at 37 °C under an
398 atmosphere of 5% CO_2/95% air. The growth plate like chondrocyte (GPLC) cell line, derived and
399 v-myc immortalized from 13DPC mouse limb buds as published[52], was obtained as a gift from Dr.
400 Vicki Rosen (Harvard School of Dental Medicine) and were grown in DMEM/F12 (Gibco) with
401 10% (v/v) FBS (Gibco) and 1% (v/v) penicillin/streptomycin at 37°C with 5% CO_2/95% air. Patient-
402 derived fibroblasts from a male *COSMC-CDG* patent (A20D-COSMC, M2)[15] were obtained as a
403 gift from Dr. Richard Cummings (Harvard Medical School) and were grown in DMEM (Gibco) with
404 10% (v/v) FBS and 1% (v/v) penicillin/streptomycin at 37°C with 5% CO_2/95% air. For routine
405 passaging, all cells listed above were detached using 0.05% trypsin-EDTA (Thermo), sub-cultured
406 every 3 to 4 days, and revived from liquid nitrogen after ≤ 10 passages.

407 **Cell line generation**

408 HEK293T cells were co-transfected with Fugene 6 (Promega) and 4 µg each of a viral envelope
409 plasmid (pMD2.g, a gift from Didier Trono and purchased from Addgene, #12259), packaging
410 plasmid (psPAX2, a gift from Didier Trono and purchased from Addgene, #12260), and Cas9
411 expression plasmid (lentiCas9-Blast, a gift from Feng Zhang and purchased from Addgene,
412 #52962) to generate Cas9 lentiviral particles. Lentiviral particles were collected from HEK293T
413 cells and filtered through a 0.45 µm syringe filter to remove cell debris before use in subsequent
414 transductions. Cas9 lentiviral particles were added to TC28a2 or GPLC wild-type cells, followed
415 by selection with blasticidin (2 µg/mL) to generate Cas9-expressing cells. To generate *COSMC*,

416 *C1GALT1*, and *CD44* knockout cell lines, sgRNAs sequences were cloned into the lentiGuide-
417 puro vector (a gift from Feng Zhang and purchased from Addgene, #52963). These constructs
418 were co-transfected with Fugene 6 into HEK293T cells along with viral plasmids pMD2.g and
419 psPAX2 to produce lentiviral particles, which were subsequently used to transduce Cas9-
420 expressing TC28a2 and GPLC cells, respectively. All sgRNA targeting sequences, and primers
421 used for genotyping, are listed in Supplementary Tables 1-2. After selection of the transduced cell
422 pool with puromycin (0.2 µg/mL) for at least 4 days, surviving cells were seeded onto a 96-well
423 plate by limiting dilution to establish clonal populations.

424 **Western blotting**

425 Total protein was extracted from cells using RIPA lysis buffer (EMD Millipore) supplemented with
426 protease inhibitors (Roche). Protein concentrations were determined by Bicinchoninic Acid (BCA)
427 assay (Thermo Scientific-Pierce). Equal amounts of protein were loaded and separated on SDS-
428 PAGE gels (4-12% Bis-Tris, NuPAGE, Invitrogen), transferred onto nitrocellulose membranes
429 (Thermo), and blocked with Intercept Blocking Buffer (LI-COR Biosciences) for 1 hour at room
430 temperature. Membranes were probed with primary antibodies against COSMC (Proteintech,
431 #19254-1-AP; 1:1,000), C1GALT1 (Santa Cruz Biotechnology, #sc-100745; 1:500), CD44 (Cell
432 Signaling Technology, #3570; 1:1000), p44/42 MAPK (ERK1/2; Cell Signaling Technology,
433 #9107; 1:1000), phospho-p44/42 MAPK (p-ERK; Cell Signaling Technology, #4370, 1:2000),
434 GAPDH (Cell Signaling Technology, #5174; 1:2500), or β-actin (Cell Signaling Technology,
435 #3700; 1:5000) at 4°C overnight. After washing with TBST, mouse and rabbit primary antibodies
436 were incubated with secondary Odyssey IR dye antibodies (anti-mouse 800, LI-COR Biosciences,
437 #926-32212; donkey anti-rabbit 680, LI-COR Biosciences, #926-68073; 1:14,000) and visualized
438 on an Odyssey infrared imaging system (LI-COR Biosciences). Band intensities were quantified
439 using ImageJ and normalized to housekeeping proteins.

440 **MAPK/ERK signaling assays**

441 For signaling assays, wild-type or knockout TC28a2 cells were cultured in 12-well plates. The
442 growth medium was exchanged for serum-free DMEM (Invitrogen) for 5 hours followed by the
443 addition of FGF2 (bFGF, Peprotech, 0- 10 ng/mL) for 5 min before placing the cells on ice. Next,
444 the cells were washed twice with ice-cold PBS and were lysed using RIPA buffer containing
445 protease inhibitors. Protein concentration was determined using the Pierce BCA Protein Assay
446 Kit (Thermo Scientific) before Western blot analysis. Cells were resolved by SDS-PAGE and
447 blotted with primary antibodies against p-ERK and ERK antibodies (Cell Signaling Technology.
448 Bands were visualized on an Odyssey Infrared imaging system (Li-Cor Biosciences). Band
449 intensities were quantitated by densitometry using Image J software.

450 **Protein biotinylation**

451 Heparin-Sepharose (100 µl, Cytiva) was pre-equilibrated with PBS (Gibco) and then loaded with
452 human FGF1 (Peprotech, #100-17A) or human FGF2 (Peprotech, #100-18B) dissolved in PBS,
453 as previously described[65]. The flow-through was collected and reloaded onto the column twice to
454 ensure complete binding. After washing twice with PBS, 0.6 mg/mL of Sulfo-NHS-LC-biotin
455 (Thermo Fisher) in PBS was applied to the column and incubated for 1 hour at room temperature.
456 Each column was washed three times with PBS, then bound biotinylated protein was eluted with
457 0.4 mL of PBS buffer containing an additional 2 M NaCl. All biotinylated proteins were stored at -
458 80 °C before use.

459 **Flow cytometry and cell surface binding experiments**

460 TC28a2 and GPLC cells were grown in monolayer culture, washed twice with PBS, and detached
461 using Accutase (Sigma-Aldrich, #A6964) via incubation for 5 min at room temperature. Cells were
462 then resuspended in PBS + 0.1% BSA (FACS buffer). For Tn and T antigen detection, 1×10^6
463 cells were pre-incubated with sialidase (Lectenz Bio, #GE0701; 50 U per 100 µL) for 1 h at 37 °C,
464 washed with FACS buffer, and stained with the VVA-FITC (Vector Labs, #FL-1231-2, 40 ng/mL),

465 anti-Tn antibody (Thermo Scientific, #MA1-80055, 1 µg/mL), or PNA lectin tagged with Alexa Fluor
466 647 (Thermo, #L32460, 20 ng/mL) for 45 min on ice in the dark.

467 For the detection of other proteins and ligands, lifted cells were incubated in suspension
468 for 30 min at 4 °C with 0.5 µg/mL mAb 10E4 (AMSBio #370255-1, Clone F58-10E4, 1:5000), 1
469 µg/mL mAb 3G10 (AMSBio, #370260-S, clone F69-3G10, 1:1000), 1 µg/mL mAb 2B6 (AMSBio
470 # 270432-CS, Clone 2B6, 1:200), 0.1 µg/mL pan-CD44 mAb (Thermo #14-0441-82, Clone IM7,
471 1:1000), 0.5 µg/mL anti-CD44v3 mAb (R&D Systems #BBA11, Clone 3G5, 1:1000), 0.2 µg/mL
472 anti-SDC1 mAb (Novus Biologicals #NB100-64980, Clone B-A38, 1:500), 0.5 µg/mL anti-SDC2
473 mAb (R&D Systems #MAB2965, Clone 305515, 1:1000), 80 nM biotin-FGF1, or 2.5 nM biotin-
474 FGF2, respectively. Where applicable, cells were pre-treated with 5 mU/mL each of heparin
475 lyases I, II, and III (BBI Solutions) for 30 min at 37 °C to generate HS neoepitopes for 3G10
476 binding, or with 2 mU/mL chondroitinase ABC (Sigma-Aldrich, #C3667-5UN) for CS neoepitope
477 detection for 2B6 binding. Bound 10E4 was detected with 2 µg/mL anti-mouse IgM AlexaFluor
478 647 (Invitrogen, #A-21238, 1:1000). Primary IgG antibodies were subsequently detected with 2
479 µg/mL anti-mouse IgG AlexaFluor 647 (Invitrogen, #A21235, 1:1000), 2 µg/mL anti-mouse IgG
480 AlexaFluor 488 (Invitrogen, #A11001, 1:1000) or 2 µg/mL anti-rat IgG AlexaFluor 488 (Invitrogen,
481 #A11006, 1:1000). Binding of biotinylated proteins was detected by streptavidin-Cy5 (Molecular
482 Probes, 1:1000). Flow cytometry was performed using a CytoFLEX S instrument (Beckman
483 Coulter; ≥10,000 events/sample). Live cells were gated based on forward and side scattering.
484 The extent of protein binding was quantified using the geometric mean of the fluorescence
485 intensity. Unstained negative controls were included in each experiment. Data were plotted and
486 analyzed in GraphPad Prism v10.8.

487 For quantification of total SDC1 protein levels by flow cytometry, monolayer cultures were
488 detached with Accutase (Sigma-Aldrich, A6964; 1 mL per 10-cm dish), fixed using 4%
489 paraformaldehyde for 20 min at room temperature, washed twice with PBS, and permeabilized
490 with 1% Triton X-100 for 5 min. After a DPBS wash, cells were blocked with 2% BSA in PBST on

491 ice for 30 min and then incubated with primary antibody against 0.2 μg/mL SDC1 (Fisher
492 Scientific, N106491010U; 1:500). After washing, cells were labeled with 2μg/mL Alexa Fluor 647-
493 conjugated anti-mouse IgG secondary antibody (Fisher, A11001; 1:1000) and analyzed via flow
494 cytometry following standard procedures.

495 **Proteoglycan cell surface recovery assays**

496 To assess recovery of cell surface SDC1 and CD44, TC28a2 wild-type, *COSMC*$^{-/-}$, and
497 *C1GALT1*$^{-/-}$ chondrocytes were plated and grown to confluence. Cells were then detached by
498 incubation with 0.25% trypsin-EDTA (Thermo, #25200056) for 15 min at 37 °C. After neutralization
499 and resuspension, 2×10^6 cells were replated and allowed to recover for the indicated times (0,
500 2, 4, 8, and 24 hours post-trypsinization). Untreated wild-type and knockout cells were maintained
501 in parallel and served as non-trypsinized controls. At each time point, cells were lifted with
502 Accutase, fixed in 4% paraformaldehyde, and analyzed for cell surface SDC1 or CD44 via flow
503 cytometry using the antibodies and methods described above. For bafilomycin A1 experiments,
504 cells were pre-treated with bafilomycin A1 (0.25 μM) or vehicle (DMSO) for 16 hours prior to flow
505 cytometry or immunofluorescence analyses.

506 **GAG isolation, purification and LC-MS disaccharide analysis**

507 2×10^6 cells were seeded into a 15 cm plate and harvested when confluent. Briefly, cells were
508 washed with PBS, lifted with trypsin (Gibco), and the trypsin-released glycosaminoglycans were
509 digested with Pronase (0.5 mg/mL, Sigma) overnight at 37 °C. The product was filtered and
510 passed through a DEAE-Sephacel (Cytiva) column equilibrated in 50 mM sodium acetate buffer,
511 pH 6.0, containing 200 mM NaCl then passed through a PD-10 desalting column (Cytiva). For HS
512 disaccharide analysis, lyophilized GAGs were incubated with 2 mU each of heparin lyases I, II,
513 and III for 16 h at 37 °C in a buffer with 40 mM ammonium acetate and 3.3 mM calcium acetate,
514 pH 7. For CS analysis, lyophilized GAGs were incubated with 50 mM Tris and 50 mM NaCl, pH

515 7.9. HS and CS disaccharides were aniline-tagged and analyzed via GRIL-LC/MS, using
516 established methods[26, 66]. All LC-MS data analysis and results are included in Supplementary
517 Tables 4-9 in the supplementary information

518 **C1GALT1 rescue experiments**

519 The sgRNA-resistant C1GALT1 cDNA vector was generated by introducing silent mutations into
520 the sgRNA target site (5'-TTTAAGCCTTATGTAAAGCA-3' mutated to 5'-
521 TTTAAGCCTTATGTTAAACA-3') in a C1GALT1 expression vector (Sino Biological, # HG19234-
522 UT). C1GALT1 cDNA was then subcloned into a pLX208-CMV-Hygro plasmid (Addgene
523 #153007). Lentiviral particles were produced in HEK293T cells by co-transfection with the
524 expression plasmid, psPAX2 packaging plasmid (Addgene #12260), and the VSV-G encoding
525 plasmid pMD2.G (Addgene #12259), as described above. Viral supernatant was collected and
526 used to transduce TC28a2 *C1GALT1*$^{-/-}$ knockout cells. Stably infected cells were selected with
527 hygromycin (75 µg/mL) for 5 days, and C1GALT1 expression was confirmed by immunoblotting.

528 **RNA extraction, qPCR, and RNA sequencing**

529 Total RNA was isolated from cells using TRIzol (Invitrogen, 15596026) and the RNeasy Kit
530 (Qiagen), following the manufacturers' instructions. cDNA synthesis was carried out with the
531 SuperScript IV First Strand Synthesis Kit (Invitrogen) using random hexamers, according to the
532 manufacturer's guidelines. Quantitative PCR was performed with cDNA and SYBR Green Master
533 Mix (Applied Biosystems) following the manufacturer's protocols. The expression levels
534 of *YWHAZ* or *Gapdh* were used to normalize the target gene expression across human and
535 mouse samples, respectively. The primers used for gene expression analyses are listed in
536 Supplementary Table 3.

537 **RNA sequencing and differential gene expression analysis**

538 For transcriptome analysis, total RNA from wild-type and knockout cell lines was used for library
539 preparation and next-generation sequencing (IGM Genomics Core, UC San Diego). Raw
540 sequencing reads were processed with the GeneGlobe RNA-seq Analysis Portal (Qiagen) to
541 remove adapters and low-quality bases, then aligned to the human genome (GRCh38;
542 GCF_000001405.38). Differential gene expression analysis was conducted within the same
543 portal, considering genes with an adjusted p-value ≤ 0.01 and a fold change of ± 2 as differentially
544 expressed. Functional annotation and gene set enrichment analysis of the top differentially
545 expressed genes were performed using Metascape (http://metascape.org/)[67].

546 **Expression and purification of human ST6GALNAC1**

547 The expression construct for human ST6GALNAC1 was generated encoding the truncated
548 domain of human ST6GALNAC1 (UniProt Q9NSC7, residues 36-600) as an NH_2-terminal fusion
549 protein in the pGEn2 expression vector, as described in prior studies[68]. Briefly, the fusion protein
550 coding region was comprised of a 25-amino acid signal sequence, an His_8 tag, AviTag, the
551 "superfolder" GFP, the 7-amino acid recognition sequence of the tobacco etch virus (TEV)
552 protease followed by the truncated ST6GALNAC1 coding region. The ST6GALNAC1 expression
553 construct was used for transient transfection of suspension culture HEK293-F cells (FreeStyle™
554 293-Fcells, Thermo Fisher Scientific) maintained at 0.5-3.0x10^6 cells/mL in a humidified CO_2
555 platform shaker incubator at 37°C with 50% relative humidity and 125 RPM. Transient transfection
556 was performed using HEK293-F cells in the expression medium comprised of a 9:1 ratio of
557 Freestyle™293 expression medium (Thermo Fisher Scientific) and EX-Cell expression medium
558 including Glutmax (Sigma-Aldrich). Transfection was initiated by the addition of plasmid DNA and
559 polyethyleneimine as transfection reagent (linear 25-kDa polyethyleneimine, Polysciences, Inc.).
560 Twenty-four hours post-transfection the cell cultures were diluted with an equal volume of fresh
561 media supplemented with valproic acid (2.2 mM final concentration) and protein production was
562 continued for an additional 5 days at 37°C, 125 RPM and 5% CO_2. Cell cultures were harvested,

563 clarified by sequential centrifugation at 1200 RPM for 10 min and 3500 RPM for 15 min at 4°C,
564 and passed through a 0.8 μM filter (Millipore, Billerica, MA). The protein preparations were
565 adjusted to contain 20 mM HEPES, 20 mM imidazole, 300 mM NaCl, pH 7.5, and subjected to
566 Ni-NTA Superflow (Qiagen, Valencia, CA) chromatography using a column preequilibrated with
567 20 mM HEPES, 300 mM NaCl, 20 mM imidazole, pH 7.5 (Buffer I). Following loading of the
568 sample, the column was washed with 3 column volumes of Buffer I followed by 3 column volumes
569 of Buffer I containing 50 mM imidazole and eluted with Buffer I containing 300 mM imidazole at
570 pH 7.0. The protein was concentrated to ~3 mg/mL using an ultrafiltration pressure cell (Millipore)
571 with a 10-kDa molecular mass cutoff membrane and further purified by size exclusion
572 chromatography using superdex 200 column, peak fractions were pooled and buffer exchanged
573 with 20 mM HEPES, 150 mM NaCl, pH7.0, 10% glycerol and adjusted at 1 mg/mL concentration.
574 The final protein preparation was aliquoted and stored at -80°C until use.

575 **Expression and purification of Sialidase from *Paenarthrobacter ureafaciens***

576 The expression cassette for sialidase from *Paenarthrobacter ureafaciens* (Uniprot Q5W7Q2:
577 residues 39-424) was generated in the pET vector. Briefly the cassette was comprised of a
578 "superfolder" GFP, an His_6 tag, followed by Sialidase coding region. The protein expression was
579 carried out in arctic express using IPTG induction (0.1 mM) overnight at 18°C. The cell pellets
580 were harvested at 8000 x g for 20 min at 4°C and further subjected for purification. The cell pellet
581 (~5 gm) was resuspended in 20-25 mL of binding buffer I (20 mM HEPES, 300 mM NaCl, 20 mM
582 imidazole, 5% glycerol, pH 7.5). The lysis was carried out using an ultrasonication probe (30
583 second pulse at an amplitude of 50 followed by cooling on ice for 1min) and the sonication
584 procedure was repeated two times (total sonication time was 6 min in each cycle). After
585 sonication, cell debris was removed by centrifugation (4°C, 12000 rpm, 30 min). The clear
586 supernatants were then diluted ten times in binding buffer and loaded on Ni-NTA superflow
587 (Qiagen, Valencia, CA) chromatography column. Following loading of the sample, the column

588 was washed with 3 column volumes of Buffer I followed by 3 column volumes of Buffer I containing
589 50 mM imidazole, and eluted with Buffer I containing 300 mM imidazole at pH 7.0. The protein
590 was concentrated to ~3 mg/mL using an ultrafiltration pressure cell (Millipore, Billerica, MA) with
591 a 10-kDa molecular mass cutoff membrane and further purified by size exclusion chromatography
592 using superdex 75 column, peak fractions were pooled and buffer exchanged with 20 mM HEPES,
593 100 mM NaCl, pH7.0, 10% glycerol, 0.05% sodium azide and adjusted at 1 mg/mL concentration.
594 The final protein preparation was aliquoted and stored at -80°C until use.

595 **Neuraminidase-coupled selective exoenzymatic labeling with ST6GALNAC1**

596 SEEL was utilized as previously described[38], with modifications. TC28a2 wild-type, *COSMC*$^{-/-}$,
597 and *C1GALT1*$^{-/-}$ cells were cultured to confluence in 10-cm dishes and washed three times with
598 5 mL PBS to remove residual serum-containing media. Cells were detached by adding PBS and
599 gently scraping with a cell scraper. Cells were pelleted and incubated for 2 hours at 37°C with
600 end-over-end rotation in 600 µL of serum-free DMEM containing recombinant ST6GALNAC1 (42
601 µg/mL), CMP-Neu5Ac-C5-triazole-biotin (100 µM, synthesized as reported[38]), BSA (2 mg/mL, 2
602 µL per 300 µL reaction), alkaline phosphatase (FastAP, Thermo Scientific, #EF0651; 2 µL per
603 300 µL reaction), and sialidase (10 µL per 300 µL). Negative control samples lacked CMP-
604 Neu5Ac-C5-triazole-biotin treatment. Cells were washed three times with 1 mL of PBS and lysed
605 in RIPA buffer containing protease inhibitors (Thermo Scientific, #88666). Cell lysates were
606 clarified by centrifugation, protein concentration was measured by the BCA assay, incubated
607 overnight at 4°C with end-over-end rotation, and adjusted for amount of Streptavidin agarose
608 beads (Thermo Scientific) to enrich biotinylated proteins. Streptavidin beads were collected on a
609 magnetic stand, supernatants were retained as flow-through, and beads were washed extensively
610 including two 1 mL washes with RIPA buffer, 1 mL high salt wash with 1M KCl in 25 mM Tris (pH
611 7.4), 1 mL high pH wash with 0.1 M Na_2CO_3 in MilliQ water, 1 mL with 2 M urea in TBS (pH 8),
612 and three 1 mL washes with RIPA buffer (1X TBS washes were included between each listed

613 wash condition). Bound proteins were eluted in 50 mM triethylammonium bicarbonate (Sigma)
614 containing 5% sodium dodecyl sulfate (Sigma) at 95°C and subjected to protein digestion and
615 processing for LC-MS/MS analysis. Eluted proteins were reduced by incubation with 10 mM of
616 dithiothreitol (Sigma) at 56°C and alkylated by 27.5 mM of iodoacetamide (Sigma) at room
617 temperature in dark. After alkylation, the proteins were trapped and washed over suspension
618 trapping columns (S-Trap micro, ProtiFi) and then digested on-column using trypsin/LysC
619 (Promega) at 37°C overnight.

620 **Secretome sample preparation**

621 Cells were seeded in 10-cm dishes and grown to confluency in DMEM supplemented with 10%
622 FBS and antibiotics. After 2 days, cells were washed three times with 5 mL PBS to remove
623 residual serum proteins. Serum-free DMEM was then added, and cells were incubated for 18
624 hours to allow protein secretion. Conditioned medium was collected and centrifuged at 1,000 × g
625 for 3 min at 4 °C to remove cell debris, and the supernatant was retained. The medium was
626 concentrated using Amicon Ultra centrifugal filters (3 kDa MWCO, 15 mL capacity) at 3,500 × g.
627 Buffer exchange into 1X TBS (pH 7.6) was performed by adding 10 mL TBS and centrifuging at
628 3,500 × g, repeated three times, with the final volume concentrated to 300 µL. The concentrated
629 secreted proteins were subsequently used for protein digestion and LC-MS/MS analysis, as
630 described above, with addition of 50 mM TEAB and SDS to utilize S-trap columns for overnight
631 protein digest with trypsin/LysC after protein reduction and alkylation.

632 **Liquid chromatography tandem mass spectrometry (LC-MS/MS) proteomics analysis**

633 Digested peptides were separated on an Acclaim PepMap RSLC C18 column (75 µm x 15 cm)
634 and eluted into the nano-electrospray ion source of an Orbitrap Eclipse™ Tribrid™ mass
635 spectrometer (Thermo Fisher Scientific) at a flow rate of 200 nL/min. The elution gradient for the
636 secretome samples consists of 1-40% acetonitrile in 0.1% formic acid over 220 minutes followed

637 by 10 minutes of 80% acetonitrile in 0.1% formic acid. The gradient for all other samples consists
638 of 1-40% acetonitrile in 0.1% formic acid over 140 minutes followed by 10 minutes of 80%
639 acetonitrile in 0.1% formic acid. The spray voltage was set to 2.2 kV and the temperature of the
640 heated capillary was set to 275 °C. Full MS scans were acquired from m/z 300 to 2000 at 60k
641 resolution, and MS/MS scans following collision-induced dissociation (CID) with the collision
642 energy at 38% were collected in the ion trap. The spectra were analyzed using SEQUEST
643 (Proteome Discoverer 2.5, Thermo Fisher Scientific) with mass tolerance set as 20 ppm for
644 precursors and 0.5 Da for fragments. The search output was filtered within the program to reach
645 a 1% false discovery rate at protein level and 10% at peptide level. The quantitation was
646 performed based on spectral counts. For secretome statistical analysis, peptide spectral counts
647 (PSM) were normalized to Normalized Spectral Abundance Factor (NSAF) and protein
648 identifications were required to be detected above a threshold of 30 total PSMs. Perseus v2.1.3
649 (Max-Planck-Institute of Biochemistry) was then used to finalize data pre-processing and
650 statistical analyses via $\log_2$ conversion of raw NSAFs with a requirement to be detected in more
651 than one biological replicate of each genotype. Proteins not found in an individual replicate were
652 assigned a value of 0. GraphPad Prism (v10.8) was then used for data visualization of differential
653 protein abundance analysis.

654 **Immunofluorescence**

655 Cells were grown on glass coverslips, washed with PBS, fixed with 4% paraformaldehyde,
656 permeabilized with 1% Triton X-100, and blocked with 2% BSA in PBST for 1 hour at room
657 temperature. Primary antibodies were applied in 2% BSA/PBST overnight at 4°C, followed by
658 three PBS washes (10 min each) and incubation with fluorescent secondary antibodies for 1 h at
659 room temperature. Coverslips were washed three times with PBS, mounted using ProLong Gold
660 antifade reagent containing DAPI (Thermo Scientific, #P36941), and sealed with clear nail polish.
661 Imaging was performed on an Olympus IX83 Confocal Microscope.

662 **Micromass differentiation of growth plate-like chondroprogenitors**

663 Immature growth plate-like chondroprogenitors (GPLCs) were maintained in DMEM/F12 (Gibco)
664 with 10% FBS (Gibco), 100 U/mL penicillin, and 100 mg/mL streptomycin sulfate (Life
665 Technologies), at 37°C with 5% CO2. For chondrogenesis assays, micromass cultures were
666 established as previously described[69] with minor modifications. Briefly, 2 x 10^5 cells were seeded
667 as a small droplet (10-30 µL) in the center of each well of a 24-well plate and incubated at 37 °C
668 with 5% CO_2 for 2 hours to facilitate cell attachment. Complete growth medium (500 µL) was then
669 gently added to the side of each well without disturbing the pellet, and cultures were incubated
670 overnight. After 24 hours, the medium was replaced with complete media + 1X insulin-transferrin-
671 selenium (ITS, Thermo Fisher) and replenished every 3 days. Chondrogenesis was evaluated on
672 Day 4 and Day 7 using Alcian Blue staining and gene expression was assessed at Day 7 via
673 quantitative PCR, as described above.

674 For Alcian Blue staining, the culture media was aspirated, and micromass cultures were
675 washed twice gently with PBS prior to fixation in 4% formaldehyde in PBS for 20 minutes at room
676 temperature. Fixed micromass cultures were then washed twice with PBS, briefly rinsed with
677 deionized water (3 minutes) and stained with 1% (w/v) Alcian Blue stain (Sigma-Aldrich, #TMS-
678 010-C) for 30 minutes at room temperature, protected from light. Excess dye was aspirated and
679 cells were rinsed extensively using deionized water. For quantification, the dye was extracted
680 overnight at room temperature with 6 M guanidine hydrochloride, and the absorbance was
681 measured at 595 nm using a plate reader.

682 **Statistics and Reproducibility**

683 Statistical tests, sample sizes, and numbers of biological replicates are provided in figure legends.
684 ****$p < 0.0001$; ***$p < 0.001$; **$p < 0.01$; *$p < 0.05$. All tests were two-sided and were performed

using Prism v10 (GraphPad). Error bars are shown to represent standard deviation from the mean. Each measurement was taken from a distinct biological sample.

Data availability

Raw data for LC-MS analysis of GAGs are available at GlycoPOST[70] under project ID GPST000656. All mass spectrometry data has been deposited to ProteomeXchange Consortium via the MassIVE partner repository (https://massive.ucsd.edu/ProteoSAFe/static/massive.jsp) with the dataset identifier MSV000099037. Raw sequencing reads and results of the RNA sequencing analysis will be made available at NCBI Gene Expression Omnibus upon publication. Any data supporting the analyses in the manuscript are available from the corresponding author upon reasonable request.

Supplementary Information

Supplementary tables, figures, and details of experimental procedures are provided in the Supporting Information.

Acknowledgements

We thank IBEX Technologies for their in-kind donation of heparin lyase enzymes. We thank Dr. Vicki Rosen (Harvard) for the gift of the GPLC cell line, and Dr. Richard Cummings for the gift of the *COSMC-CDG* patient fibroblast line (A20D-COSMC, M2). Recombinant ST6GALNAC1 and neuraminidase were kindly provided by Dr. Kelley Moremen (UGA). We thank Dr. Hans Wandall (University of Copenhagen) for helpful discussions regarding *O*-GalNac glycosylation and proteomics experiments. We also thank the GlycoAnalytics Core Facility at University of California, San Diego for help with analytical experiments. This work was supported by NIH grants to R.J.W. (NIAMS R21AR080957, NIGMS R35GM150736) and the NSF BioFoundry: Glycoscience Research, Education, and Training (BioF:GREAT, 240020, to L.W.). This publication includes RNA-seq data generated at the UC San Diego IGM Genomics Center utilizing

an Illumina NovaSeq 6000 that was purchased with funding from a National Institutes of Health SIG grant (#S10 OD026929). Certain figure panels (Figs. 2A, 4A, 6A, 8, and Suppl.Fig. 1D, 4B) were created in BioRender.

Author Contributions

Unless otherwise noted, X.D. performed the experimental work and analyzed the data. S.B. and P.Z. generated, processed, and analyzed the proteomics data. K.G. and K.S. generated and characterized the CD44 knockout cells and performed immunoblotting and qPCR experiments. A.B. generated, processed, and analyzed the LC-MS GAG compositional data. D.C. generated recombinant ST6GALNAC1 and sialidase for SEEL experiments. X.D., L.W., and R.J.W. wrote the paper, with input from all listed co-authors.

Competing Interests

The authors declare no competing interests.

721 **Figure Legends**

722 **Figure 1. Genetic ablation of *COSMC/C1GALT1* reduces cell surface heparan sulfate in**
723 **TC28a2 chondrocytes.** (A) Schematic of mucin-type *O*-GalNAcylation. Polypeptide GalNAc-
724 transferases (ppGalNAc-Ts/GALNTs; ~20 isoenzymes) initiate addition of GalNAc to serine or
725 threonine residues of core proteins. Loss of COSMC or C1GALT1 blocks core 1 extension (T
726 antigen), resulting in accumulation of truncated *O*-glycans (Tn antigen). VVA lectin detects Tn
727 antigen, whereas PNA lectin detects T antigen. Western blot validation of (B) *COSMC*$^{-/-}$ and (C)
728 *C1GALT1*$^{-/-}$ knockout cell lines; GAPDH serves as a loading control. (D-E) Flow cytometry
729 analysis of VVA and PNA lectin to wild-type and COSMC/C1GALT1 knockout cells. (F-G) LC-MS
730 quantification of total cell surface heparan sulfate (HS) and chondroitin sulfate (CS) levels. (H)
731 Schematic of GAG-specific antibodies: 3G10 recognizes HS stubs generated by heparin lyase
732 and 2B6 detects CS stubs generated by chondroitinase ABC. (I) Flow cytometry analysis of 3G10
733 binding in wild-type and knockout cells. (J) Flow cytometry analysis of 2B6 binding in wild-type
734 and knockout cells. Data points are shown as mean ± SD (n ≥ 3 independent experiments); p-
735 values were determined by one-way ANOVA with Tukey post-test with ****$p < 0.0001$, *** $p <$
736 0.001, ** $p < 0.01$, * $p < 0.05$.

737 **Figure 2. Truncation of *O*-GalNAc glycans disrupts FGF binding and downstream**
738 **MAPK/ERK signaling.** (A) Diagram of the FGF-FGFR-heparan sulfate ternary complex, whch
739 regulates downstream pathways including MAPK/ERK signaling. (B-C) FGF1 and FGF2 ligand
740 binding were significantly reduced in knockout cells versus wild-type control cells. (D) Cell surface
741 expression of FGFR1 was unchanged in wild-type and knockout cells, as quantified via flow
742 cytometry. (E) Western blot analysis of FGF2 induced ERK phosphorylation (p-ERK) and total
743 ERK (t-ERK) levels in wild-type and knockout cells. (F) Western blot band intensities were
744 quantitated by densitometry and plotted as the ratio of p-ERK to t-ERK signal. (G) Western blot
745 analysis of C1GALT1 protein levels upon reintroduction of human C1GALT1 (hC1GALT1) into

746 *C1GALT1*$^{-/-}$ cells. (H) Flow cytometry analysis of FGF2 binding in wild-type, *C1GALT1*$^{-/-}$, and
747 *C1GALT1*$^{-/-}$ cells transduced with *C1GALT1* cDNA. (I) Flow cytometry analysis of HS stubs using
748 3G10 antibody, and FGF binding in A20D-*COSMC-CDG* patient fibroblasts. Data points are
749 shown as mean ± SD (n ≥ 3 independent experiments); p-values were determined by one-way
750 ANOVA with Tukey post-test (A-H) and student's T-tests (I) with ****p < 0.0001, *** p < 0.001, **
751 p < 0.01, * p < 0.05.

752 **Figure 3. Transcriptome analysis of *COSMC*$^{-/-}$ and *C1GALT1*$^{-/-}$ knockout cells reveals**
753 **altered expression of extracellular matrix and proteoglycan genes.** Venn diagrams
754 comparing significantly downregulated (A) and upregulated (B) genes (Fold change ≥ 2, FDR p ≤
755 0.01) from RNA-seq datasets for *COSMC*$^{-/-}$ and *C1GALT1*$^{-/-}$ knockout cells. Gene Ontology
756 enrichment analysis of overlapping 128 downregulated (C) and 219 upregulated (D) genes shared
757 in *COSMC*$^{-/-}$ and *C1GALT1*$^{-/-}$ cells. (E) Differential expression analysis of proteoglycan and GAG
758 biosynthetic genes (FDR p ≤ 0.01) compared to wild-type control cells. Flow cytometry analysis
759 of (F) syndecan-1 (SDC1) and (G) syndecan-2 levels in TC28a2 wild-type, *COSMC*$^{-/-}$, and
760 *C1GALT1*$^{-/-}$ cells. Data points are shown as mean ± SD (n ≥ 3 independent experiments); p-
761 values were determined by one-way ANOVA with Tukey post-test with **** p < 0.0001, *** p <
762 0.001, ** p < 0.01, * p < 0.05.

763 **Figure 4. Truncation of *O*-GalNAc glycans leads to remodeling of the secreted**
764 **glycoproteome in TC28a2 chondrocytes.** (A) Workflow for analysis of the secretome from
765 TC28a2 wild-type, *COSMC*$^{-/-}$, and *C1GALT1*$^{-/-}$ cells. (B) Venn diagram showing the overlapping
766 protein hits identified in the secretome analysis of *COSMC*$^{-/-}$ and *C1GALT1*$^{-/-}$ cells versus wild-
767 type controls (n = 3 independent experiments). Over half of the identified protein hits were shared
768 between the knockout cell lines. Volcano plots showing proteins significantly altered in
769 abundance in (C) *COSMC*$^{-/-}$ and (D) *C1GALT1*$^{-/-}$ cells versus wild-type controls. Proteins were
770 categorized and highlighted as *Proteoglycans*, *O-GalNAcylated proteins*, *Proteases*, *ECM*

771 *remodeling enzymes*, *Growth factors/cytokines/signaling proteins*, and *other proteins*. p-values
772 were determined by Student t-test, and significantly altered proteins were identified using a
773 threshold of $p \leq 0.05$.

774 **Figure 5. Loss of extended *O*-GalNAc glycans decreases SDC1 cell surface stability and**
775 **enhances its lysosomal degradation.** (A) Time course quantification of cell surface SDC1 levels
776 via flow cytometry prior to and after trypsinization (0-24 hours). Data is normalized to untreated
777 wild-type cells (dashed line). (B) Quantification of SDC1 recovery to the cell surface. Data were
778 normalized to the respective untreated control for each genotype and fitted using linear
779 regression. Table inset includes slopes ± SD for each. Statistical comparisons were performed
780 using an F-test to compare the slopes of knockout lines versus wild-type cells (* $p < 0.05$). (C)
781 Quantification of total SDC1 protein levels in wild-type, *COSMC*$^{-/-}$, and *C1GALT1*$^{-/-}$ cells treated
782 with bafilomycin A1 (0.25 μM) or DMSO vehicle for 16 hours. (D) Representative histograms from
783 flow cytometry analysis of total SDC1 levels in cells treated with bafilomycin A1. (E) Flow
784 cytometry analysis of cell surface SDC1 levels after treatment with bafilomycin A1 or DMSO
785 vehicle. Data points are shown as mean ± SD ($n \geq 3$ independent experiments); p-values were
786 determined by one-way ANOVA with Tukey post-test (A,C), and student's T-test (E) with **** $p <$
787 0.0001, *** $p < 0.001$, ** $p < 0.01$, * $p < 0.05$.

788 **Figure 6. Complex *O*-GalNAc glycans stabilize CD44 and regulate CD44v3-FGF binding.** (A)
789 Schematic representation of CD44 protein structure. CD44 is extensively *O*-glycosylated, and
790 alternative splicing generates multiple isoforms, with CD44v3 bearing a heparan sulfate chain that
791 can mediate FGF binding. (B) Western blotting and (C) quantification of CD44 protein levels using
792 a pan-CD44 antibody in TC28a2 wild-type, *COSMC*$^{-/-}$, and *C1GALT1*$^{-/-}$ cells, normalized to
793 GAPDH ($n = 3$ independent experiments). (D) Reintroduction of hC1GALT1 restored cell surface
794 CD44 levels in *C1GALT1*$^{-/-}$ knockout cells. (E) Detection and quantification of cell surface CD44v3
795 levels in wild-type and mutant lines using an anti-CD44v3 antibody and flow cytometry. (F)

796 Validation of TC28a2 *CD44*$^{-/-}$ knockout cells via Western blot using a pan-CD44 antibody. Flow
797 cytometry analyses of cell surface CD44v3 levels, (H) 3G10 binding, and (I) FGF1 and (J) FGF2
798 binding in wild-type and *CD44*$^{-/-}$ cells. Data points are shown as mean ± SD (n ≥ 3 independent
799 experiments); p-values were determined by one-way ANOVA with Tukey post-test (C-E), and
800 student's T-test (G-J) with **** $p < 0.0001$, *** $p < 0.001$, ** $p < 0.01$, * $p < 0.05$.

801 **Figure 7. Disruption of *O*-GalNAc glycosylation impairs chondrogenic maturation and**
802 **cartilage matrix elaboration in growth plate-like chondroprogenitors.** Flow cytometry
803 analysis of (A) VVA lectin, (B) PNA lectin, (C) 3G10 antibody, (D) FGF1, (E) FGF2, and (F) pan-
804 CD44 antibody binding in wild-type and knockout growth-plate-like chondroprogenitors (GPLCs).
805 (G) Micromass cultures of GPLC wild-type, *Cosmc*$^{-/-}$, and *C1galt1*$^{-/-}$ cells at day 4 and day 7 after
806 chondrogenic induction with insulin-transferrin-selenium (ITS). At each time point, cultures were
807 fixed and stained with Alcian blue. (H) Quantification of Alcian blue staining confirmed visual data
808 and confirmed statistical significance at Day 7. qPCR analysis of chondrogenic markers (I) *Acan*
809 (J) *Col2a1*, and (K) *Sox9* in wild-type and knockout GPLC micromass cultures at Day 7. Data
810 points are shown as mean ± SD (n ≥ 3 independent experiments); p-values were determined by
811 one-way ANOVA with Tukey post-test with **** $p < 0.0001$, *** $p < 0.001$, ** $p < 0.01$.

812 **Figure 8. Proposed model of proteoglycan homeostasis and ECM remodeling alterations**
813 **caused by truncation of *O*-GalNAc glycans in *COSMC/C1GALT1*-deficient cells.**

814 **Supplementary Figure 1. Validation and characterization of TC28a2 *COSMC*$^{-/-}$ and**
815 ***C1GALT1*$^{-/-}$ knockout clones.** CRISPR sgRNA targeting of human (A) *COSMC* and (B)
816 *C1GALT1* in TC28a2 chondrocytes. Frameshift biallelic mutations in clonal cell lines for Exon 1
817 of *COSMC* and Exon 2 of *C1GALT1* were confirmed by Sanger sequencing. (C) Flow cytometry
818 analysis of anti-Tn antibody binding to wild-type and *COSMC/C1GALT1* knockout cells (n = 3
819 independent experiments). (D) Workflow for isolation, purification, enzymatic digestion, aniline

820 tagging, and LC-MS analysis of glycosaminoglycans. GRIL-LC-MS analysis of (E) HS
821 disaccharides, (F) HS sulfates per disaccharide, and (G) HS sulfation in wild-type, *COSMC*$^{-/-}$, and
822 *C1GALT1*$^{-/-}$ knockout lines (n = 4 independent experiments). GRIL-LC-MS analysis of (H) CS/DS
823 disaccharides and (I) CS/DS sulfation of wild-type and knockout cells (n ≥ 3 independent
824 experiments). Data points are shown as mean ± SD; p-values were determined by student t-test
825 with **** p < 0.0001, *** p < 0.001, ** p < 0.01, * p < 0.05.

826 **Supplementary Figure 2. Validation and characterization of additional TC28a2 *COSMC*^{c6}**
827 **and *C1GALT1*^{t2} knockout clones.** Validation of CRISPR targeting for additional (A) *COSMC*
828 (COSMC^{c6}) and (B) *C1GALT1* (C1GALT1^{t2}) knockout clones. Frameshift biallelic mutations were
829 confirmed by Sanger sequencing. Flow cytometry analysis of (C) PNA lectin, (D) VVA lectin, (E)
830 anti-Tn antibody, (F) 3G10, (G) FGF1, and (H) FGF2 binding in COSMC^{c6}and C1GALT1^{t2}
831 knockout clones compared with wild-type control cells. Data points are shown as mean ± SD (n
832 ≥ 3independent experiments); p-values were determined by one-way ANOVA with Tukey post-
833 test with ****p < 0.0001, *** p < 0.001, ** p < 0.01, * p < 0.05.

834 **Supplementary Figure 3. RNA-seq data analysis and qPCR validation experiments.** (A) PCA
835 analysis reveals distinct clustering of TC28a2 wild-type, *COSMC*$^{-/-}$, and *C1GALT1*$^{-/-}$ triplicate
836 samples. (B) Hierarchical clustering and differential expression analysis of triplicate RNA-seq
837 datasets. (C) qPCR validation of gene expression changes in additional COSMC^{c6} and
838 C1GALT1^{t2} knockout clones. Data points are shown as mean ± SD (n = 3 independent
839 experiments); p-values were determined by one-way ANOVA with Tukey post-test with **** p <
840 0.0001, *** p < 0.001, ** p < 0.01, * p < 0.05.

841 **Supplementary Figure 4. One-step Selective exoenzymatic labeling (SEEL) with**
842 **ST6GALNAC1**. (A) Commasie stained SDS-PAGE gel for purified recombinant human
843 ST6GALNAC1-GFP fusion protein. (B) Schematic of one-step SEEL labeling of TC28a2 cells with

844 ST6GALNAC1 and CMP-Neu5Ac-C5-triazole-biotin. (C) Representative western blot showing
845 streptavidin enrichment versus flow through from SEEL labeling of *COSMC*$^{-/-}$ and *C1GALT1*$^{-/-}$
846 cells. The one-step SEEL reactions with ST6GALNAC1 were performed as described in the
847 Methods section. (D) The SEEL labeling method detected a number of known *O*-GalNAcylated
848 glycoproteins (black), including multiple heparan sulfate proteoglycans (blue).

849 **Supplementary Figure 5. Immunofluorescence images of SDC1 staining in TC28a2**
850 **chondrocytes.** (A) Representative confocal images of SDC1 (red) and nuclei (DAPI; blue) in
851 DMSO-treated cells. The scale bar represents 20 nm. (B) Quantification of SDC1 fluorescence
852 intensity using ImageJ. (C) Representative confocal images of SDC1 (red) and nuclei (DAPI; blue)
853 in cells after treatment with bafilomycin A1 (250 nM) for 16 hours. The scale bar represents 20
854 nm. (B) Quantification of SDC1 fluorescence intensity in bafilomycin A1-treated cells versus wild-
855 type controls. Data points are shown as mean ± SD (n = 25-35 cells from three independent
856 biological replicates); p-values were determined by one-way ANOVA with Tukey post-test with
857 **** $p < 0.0001$.

858 **Supplementary Figure 6. Anti-CD44 binding assays and *CD44*$^{-/-}$ knockout clone validation.**
859 (A) Flow cytometry analysis of cell surface CD44 levels in *COSMC*^{c6} and *C1GALT1*^{t2} knockout
860 clones. (B) Time course quantification of cell surface CD44 levels via flow cytometry prior to and
861 after trypsinization (0-24 hours). Data is normalized to untreated wild-type cells. Data points are
862 shown as mean ± SD (n = 3 independent experiments); p-values were determined by one-way
863 ANOVA with Tukey post-test with **** $p < 0.0001$, *** $p < 0.001$, ** $p < 0.01$, * $p < 0.05$. (C) CRISPR
864 sgRNA targeting of human *CD44* in TC28a2 chondrocytes. (C) Frameshift biallelic mutations in a
865 clonal cell line for Exon 5 of *CD44* were confirmed by Sanger sequencing.

866 **Supplementary Figure 7. Validation of murine GPLC *Cosmc*$^{-/-}$ and *C1galt1*$^{-/-}$ knockout**
867 **clones.** CRISPR sgRNA targeting of mouse (A) *Cosmc* and (B) *C1galt1* in murine growth plate-

868 like chondroprogenitors (GPLCs). Frameshift biallelic mutations in a clonal cell line for Exon 1 of

869 *Cosmc* and Exon 2 of *C1galt1* were confirmed by Sanger sequencing.

870 **References**

871

872 1. Rocamora F*, et al.* Glycosylation shapes the efficacy and safety of diverse protein, gene
873 and cell therapies. *Biotechnol Adv* **67**, 108206 (2023).

874

875 2. He M, Zhou X, Wang X. Glycosylation: mechanisms, biological functions and clinical
876 implications. *Signal transduction and targeted therapy* **9**, 194 (2024).

877

878 3. Huang YF*, et al.* Global mapping of glycosylation pathways in human-derived cells. *Dev*
879 *Cell* **56**, 1195-1209.e1197 (2021).

880

881 4. Tang X*, et al.* Transcriptomic and glycomic analyses highlight pathway-specific
882 glycosylation alterations unique to Alzheimer's disease. *Scientific reports* **13**, 7816
883 (2023).

884

885 5. Reily C, Stewart TJ, Renfrow MB, Novak J. Glycosylation in health and disease. *Nature*
886 *Reviews Nephrology* **15**, 346-366 (2019).

887

888 6. Wandall HH, Nielsen MAI, King-Smith S, de Haan N, Bagdonaite I. Global functions of
889 O-glycosylation: promises and challenges in O-glycobiology. *FEBS J* **288**, 7183-7212
890 (2021).

891

892 7. Zhang Y*, et al.* A Sweet Warning: Mucin-Type O-Glycans in Cancer. *Cells* **11**, (2022).

893

894 8. Radhakrishnan P*, et al.* Immature truncated O-glycophenotype of cancer directly
895 induces oncogenic features. *Proceedings of the National Academy of Sciences* **111**,
896 E4066-E4075 (2014).

897

898 9. Sun X, Tie HC, Chen B, Lu L. Glycans function as a Golgi export signal to promote the
899 constitutive exocytic trafficking. *J Biol Chem* **295**, 14750-14762 (2020).

900

901 10. Basu A, Patel NG, Nicholson ED, Weiss RJ. Spatiotemporal diversity and regulation of
902 glycosaminoglycans in cell homeostasis and human disease. *Am J Physiol Cell Physiol*
903 **322**, C849-c864 (2022).

904

905 11. Weiss RJ, Esko JD, Tor Y. Targeting heparin and heparan sulfate protein interactions.
906 *Org Biomol Chem* **15**, 5656-5668 (2017).

907

908 12. Xu D, Esko JD. Demystifying heparan sulfate-protein interactions. *Annu Rev Biochem*
909 **83**, 129-157 (2014).

910

911 13. Alcaide-Ruggiero L, Cugat R, Domínguez JM. Proteoglycans in Articular Cartilage and
912 Their Contribution to Chondral Injury and Repair Mechanisms. *Int J Mol Sci* **24**, (2023).

14. Matsumoto K, Irie F, Mackem S, Yamaguchi Y. A mouse model of chondrocyte-specific somatic mutation reveals a role for Ext1 loss of heterozygosity in multiple hereditary exostoses. *Proceedings of the National Academy of Sciences* **107**, 10932-10937 (2010).

15. Erger F*, et al.* Germline C1GALT1C1 mutation causes a multisystem chaperonopathy. *Proc Natl Acad Sci U S A* **120**, e2211087120 (2023).

16. Granjo P*, et al.* Mapping the diagnostic odyssey of congenital disorders of glycosylation (CDG): insights from the community. *Orphanet J Rare Dis* **19**, 407 (2024).

17. Bukowska-Olech E*, et al.* Hereditary Multiple Exostoses-A Review of the Molecular Background, Diagnostics, and Potential Therapeutic Strategies. *Front Genet* **12**, 759129 (2021).

18. Yoshida CA*, et al.* Overexpression of Galnt3 in chondrocytes resulted in dwarfism due to the increase of mucin-type O-glycans and reduction of glycosaminoglycans. *J Biol Chem* **289**, 26584-26596 (2014).

19. Steentoft C*, et al.* Precision mapping of the human O-GalNAc glycoproteome through SimpleCell technology. *Embo j* **32**, 1478-1488 (2013).

20. Goldring MB*, et al.* Interleukin-1 beta-modulated gene expression in immortalized human chondrocytes. *J Clin Invest* **94**, 2307-2316 (1994).

21. Loeser RF, Shanker G, Carlson CS, Gardin JF, Shelton BJ, Sonntag WE. Reduction in the chondrocyte response to insulin-like growth factor 1 in aging and osteoarthritis: studies in a non-human primate model of naturally occurring disease. *Arthritis Rheum* **43**, 2110-2120 (2000).

22. Bennett EP, Mandel U, Clausen H, Gerken TA, Fritz TA, Tabak LA. Control of mucin-type O-glycosylation: A classification of the polypeptide GalNAc-transferase gene family. *Glycobiology* **22**, 736-756 (2012).

23. Nielsen MI*, et al.* Global mapping of GalNAc-T isoform-specificities and O-glycosylation site-occupancy in a tissue-forming human cell line. *Nat Commun* **13**, 6257 (2022).

24. Bagdonaite I*, et al.* O-glycan initiation directs distinct biological pathways and controls epithelial differentiation. *EMBO Rep* **21**, e48885 (2020).

25. Basu A*, et al.* Quantitative HILIC-Q-TOF-MS Analysis of Glycosaminoglycans and Non-reducing End Carbohydrate Biomarkers via Glycan Reductive Isotopic Labeling. *Anal Chem* **97**, 17490-17500 (2025).

957
958 26. Lawrence R*, et al.* Evolutionary differences in glycosaminoglycan fine structure detected
959 by quantitative glycan reductive isotope labeling. *J Biol Chem* **283**, 33674-33684 (2008).

960
961 27. David G, Bai XM, Van der Schueren B, Cassiman JJ, Van den Berghe H. Developmental
962 changes in heparan sulfate expression: in situ detection with mAbs. *J Cell Biol* **119**, 961-
963 975 (1992).

964
965 28. Bayliss MT, Osborne D, Woodhouse S, Davidson C. Sulfation of chondroitin sulfate in
966 human articular cartilage - The effect of age, topographical position, and zone of
967 cartilage on tissue composition. *J Biol Chem* **274**, 15892-15900 (1999).

968
969 29. Pellegrini L. Role of heparan sulfate in fibroblast growth factor signalling: a structural
970 view. *Curr Opin Struct Biol* **11**, 629-634 (2001).

971
972 30. Xie Y*, et al.* FGF/FGFR signaling in health and disease. *Signal Transduct Target Ther* **5**,
973 181 (2020).

974
975 31. Schultz V*, et al.* Heparan Sulfate Domains Required for Fibroblast Growth Factor 1 and
976 2 Signaling through Fibroblast Growth Factor Receptor 1c. *J Biol Chem* **292**, 2495-2509
977 (2017).

978
979 32. Iozzo RV, Schaefer L. Proteoglycan form and function: A comprehensive nomenclature
980 of proteoglycans. *Matrix Biol* **42**, 11-55 (2015).

981
982 33. Arrington CB, Peterson AG, Yost HJ. Sdc2 and Tbx16 regulate Fgf2-dependent
983 epithelial cell morphogenesis in the ciliated organ of asymmetry. *Development* **140**,
984 4102-4109 (2013).

985
986 34. Zhang J, Wang Y. Emerging roles of O-GlcNAcylation in protein trafficking and
987 secretion. *J Biol Chem* **300**, 105677 (2024).

988
989 35. Zhang L, Syed ZA, van Dijk Härd I, Lim JM, Wells L, Ten Hagen KG. O-glycosylation
990 regulates polarized secretion by modulating Tango1 stability. *Proc Natl Acad Sci U S A*
991 **111**, 7296-7301 (2014).

992
993 36. Chia J, Goh G, Bard F. Short O-GalNAc glycans: regulation and role in tumor
994 development and clinical perspectives. *Biochimica et Biophysica Acta (BBA) - General*
995 *Subjects* **1860**, 1623-1639 (2016).

996
997 37. Vakhrushev SY, Steentoft C, Vester-Christensen MB, Bennett EP, Clausen H, Levery
998 SB. Enhanced Mass Spectrometric Mapping of the Human GalNAc-type O-
999 Glycoproteome with SimpleCells. *Mol Cell Proteomics* **12**, 932-944 (2013).

38. Sun T, *et al.* One-Step Selective Exoenzymatic Labeling (SEEL) Strategy for the Biotinylation and Identification of Glycoproteins of Living Cells. *J Am Chem Soc* **138**, 11575-11582 (2016).

39. Ikehara Y, *et al.* Cloning and expression of a human gene encoding an N-acetylgalactosamine-α2,6-sialyltransferase (ST6GalNAc I): a candidate for synthesis of cancer-associated sialyl-Tn antigens. *Glycobiology* **9**, 1213-1224 (1999).

40. Steentoft C, *et al.* Precision mapping of the human O-GalNAc glycoproteome through SimpleCell technology. *The EMBO journal* **32**, 1478-1488 (2013).

41. Malaker SA, *et al.* Revealing the human mucinome. *Nature communications* **13**, 3542 (2022).

42. Yin X, Bern M, Xing Q, Ho J, Viner R, Mayr M. Glycoproteomic analysis of the secretome of human endothelial cells. *Mol Cell Proteomics* **12**, 956-978 (2013).

43. Almeida-Marques C, *et al.* Secretome processing for proteomics: A methods comparison. *Proteomics* **24**, e2300262 (2024).

44. Pedersen NB, *et al.* Low density lipoprotein receptor class A repeats are O-glycosylated in linker regions. *J Biol Chem* **289**, 17312-17324 (2014).

45. Wang S, *et al.* Site-specific O-glycosylation of members of the low-density lipoprotein receptor superfamily enhances ligand interactions. *J Biol Chem* **294**, 8349 (2019).

46. Burbach BJ, Friedl A, Mundhenke C, Rapraeger AC. Syndecan-1 accumulates in lysosomes of poorly differentiated breast carcinoma cells. *Matrix Biol* **22**, 163-177 (2003).

47. Yocum SA, Lopresti-Morrow LL, Gabel CA, Milici AJ, Mitchell PG. Bafilomycin A1 inhibits IL-1-stimulated proteoglycan degradation by chondrocytes without affecting stromelysin synthesis. *Arch Biochem Biophys* **316**, 827-835 (1995).

48. Lin NY, *et al.* Truncation of GalNAc-type O-glycans Suppresses CD44-mediated Osteoclastogenesis and Bone Metastasis in Breast Cancer. *Mol Cancer Res* **21**, 664-674 (2023).

49. Knudson CB. Hyaluronan and CD44: strategic players for cell-matrix interactions during chondrogenesis and matrix assembly. *Birth Defects Res C Embryo Today* **69**, 174-196 (2003).

1043 50. Xu Y, Wang A-T, Xiao J-H. CD44 mediates hyaluronan to promote the differentiation of
1044 human amniotic mesenchymal stem cells into chondrocytes. *Biotechnology Letters* **45**,
1045 411-422 (2023).

1046
1047 51. Zhen Y, Haugsten EM, Singh SK, Wesche J. Proximity Labeling by a Recombinant
1048 APEX2-FGF1 Fusion Protein Reveals Interaction of FGF1 with the Proteoglycans CD44
1049 and CSPG4. *Biochemistry* **57**, 3807-3816 (2018).

1050
1051 52. Rosen V*, et al.* Development of immortalized cells derived from 13DPC mouse limb buds
1052 as a system to study the effects of recombinant human bone morphogenetic protein-2
1053 (rhBMP-2) on limb bud cell differentiation. *Prog Clin Biol Res* **383a**, 305-315 (1993).

1054
1055 53. Rosen V, Nove J, Song JJ, Thies RS, Cox K, Wozney JM. Responsiveness of clonal
1056 limb bud cell lines to bone morphogenetic protein 2 reveals a sequential relationship
1057 between cartilage and bone cell phenotypes. *J Bone Miner Res* **9**, 1759-1768 (1994).

1058
1059 54. Underhill TM, Dranse HJ, Hoffman LM. Analysis of chondrogenesis using micromass
1060 cultures of limb mesenchyme. *Methods Mol Biol* **1130**, 251-265 (2014).

1061
1062 55. Yoon BS*, et al.* BMPs regulate multiple aspects of growth-plate chondrogenesis through
1063 opposing actions on FGF pathways. *Development* **133**, 4667-4678 (2006).

1064
1065 56. Song H, Park K-H. Regulation and function of SOX9 during cartilage development and
1066 regeneration. *Seminars in Cancer Biology* **67**, 12-23 (2020).

1067
1068 57. Alfalah M, Jacob R, Preuss U, Zimmer KP, Naim H, Naim HY. O-linked glycans mediate
1069 apical sorting of human intestinal sucrase-isomaltase through association with lipid rafts.
1070 *Curr Biol* **9**, 593-596 (1999).

1071
1072 58. Altschuler Y*, et al.* Clathrin-mediated endocytosis of MUC1 is modulated by its
1073 glycosylation state. *Mol Biol Cell* **11**, 819-831 (2000).

1074
1075 59. Kato K*, et al.* Polypeptide GalNAc-transferase T3 and familial tumoral calcinosis.
1076 Secretion of fibroblast growth factor 23 requires O-glycosylation. *J Biol Chem* **281**,
1077 18370-18377 (2006).

1078
1079 60. Yeaman C, Gall AHL, Baldwin AN, Monlauzeur L, Bivic AL, Rodriguez-Boulan E. The O-
1080 glycosylated Stalk Domain Is Required for Apical Sorting of Neurotrophin Receptors in
1081 Polarized MDCK Cells. *Journal of Cell Biology* **139**, 929-940 (1997).

1082
1083 61. Sammon D*, et al.* Molecular mechanism of decision-making in glycosaminoglycan
1084 biosynthesis. *Nature communications* **14**, 6425 (2023).

1085

1086 62. Springer GF. T and Tn, general carcinoma autoantigens. *Science* **224**, 1198-1206
1087 (1984).

1088
1089 63. Cervoni GE, Cheng JJ, Stackhouse KA, Heimburg-Molinaro J, Cummings RD. O-glycan
1090 recognition and function in mice and human cancers. *Biochem J* **477**, 1541-1564 (2020).

1091
1092 64. Theocharis AD, Karamanos NK. Proteoglycans remodeling in cancer: Underlying
1093 molecular mechanisms. *Matrix Biol*, (2017).

1094
1095 65. Basu A, Weiss RJ. Glycosaminoglycan Analysis: Purification, Structural Profiling, and
1096 GAG-Protein Interactions. *Methods Mol Biol* **2597**, 159-176 (2023).

1097
1098 66. Basu A*, et al.* Quantitative HILIC-Q-TOF-MS Analysis of Glycosaminoglycans and Non-
1099 reducing End Carbohydrate Biomarkers via Glycan Reductive Isotopic Labeling.
1100 *Analytical Chemistry* **97**, 17490-17500 (2025).

1101
1102 67. Zhou Y*, et al.* Metascape provides a biologist-oriented resource for the analysis of
1103 systems-level datasets. *Nat Commun* **10**, 1523 (2019).

1104
1105 68. Moremen KW*, et al.* Expression system for structural and functional studies of human
1106 glycosylation enzymes. *Nat Chem Biol* **14**, 156-162 (2018).

1107
1108 69. Greco KV*, et al.* High density micromass cultures of a human chondrocyte cell line: A
1109 reliable assay system to reveal the modulatory functions of pharmacological agents.
1110 *Biochemical pharmacology* **82**, 1919-1929 (2011).

1111
1112 70. Watanabe Y, Aoki-Kinoshita KF, Ishihama Y, Okuda S. GlycoPOST realizes FAIR
1113 principles for glycomics mass spectrometry data. *Nucleic Acids Res* **49**, D1523-d1528
1114 (2021).

1115

Figure 1

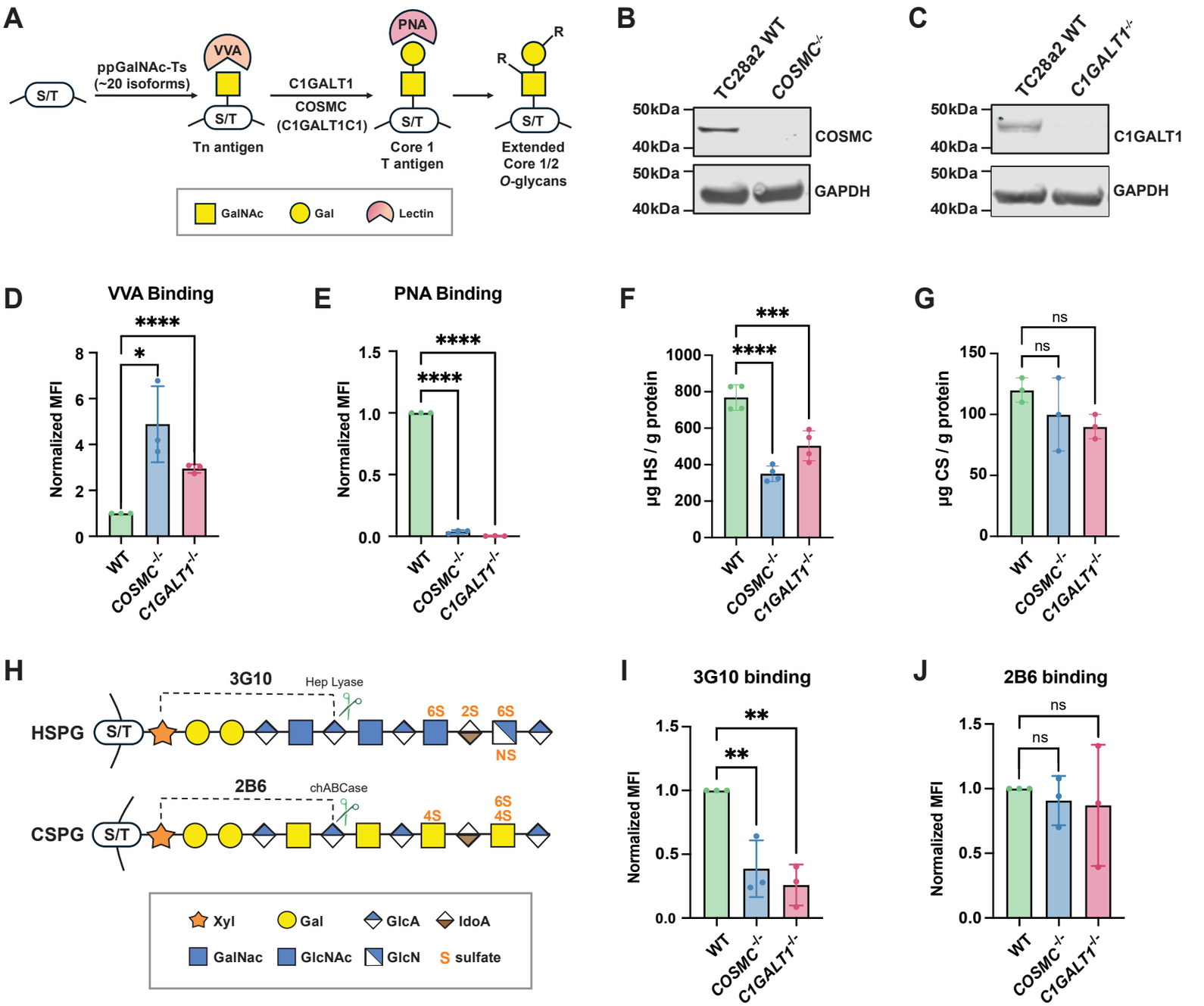
A
S/T
ppGalNAc-Ts
(~20 isoforms)
VVA
S/T
Tn antigen
C1GALT1
COSMC
(C1GALT1C1)
PNA
S/T
Core 1
T antigen
R
R
S/T
Extended
Core 1/2
O-glycans
GalNAc
Gal
Lectin
B
TC28a2 WT
COSMC-/-
50kDa
40kDa
COSMC
50kDa
40kDa
GAPDH
C
TC28a2 WT
C1GALT1-/-
50kDa
40kDa
C1GALT1
50kDa
40kDa
GAPDH
D
VVA Binding
Normalized MFI
****
*
WT
COSMC-/-
C1GALT1-/-
E
PNA Binding
Normalized MFI
****
****
WT
COSMC-/-
C1GALT1-/-
F
µg HS / g protein
***
****
WT
COSMC-/-
C1GALT1-/-
G
µg CS / g protein
ns
ns
WT
COSMC-/-
C1GALT1-/-
H
3G10
Hep Lyase
HSPG
S/T
6S
2S
6S
NS
2B6
chABCase
CSPG
S/T
4S
6S
4S
Xyl
Gal
GlcA
IdoA
GalNac
GlcNAc
GlcN
S sulfate
I
3G10 binding
Normalized MFI
**
**
WT
COSMC-/-
C1GALT1-/-
J
2B6 binding
Normalized MFI
ns
ns
WT
COSMC-/-
C1GALT1-/-

Figure 2

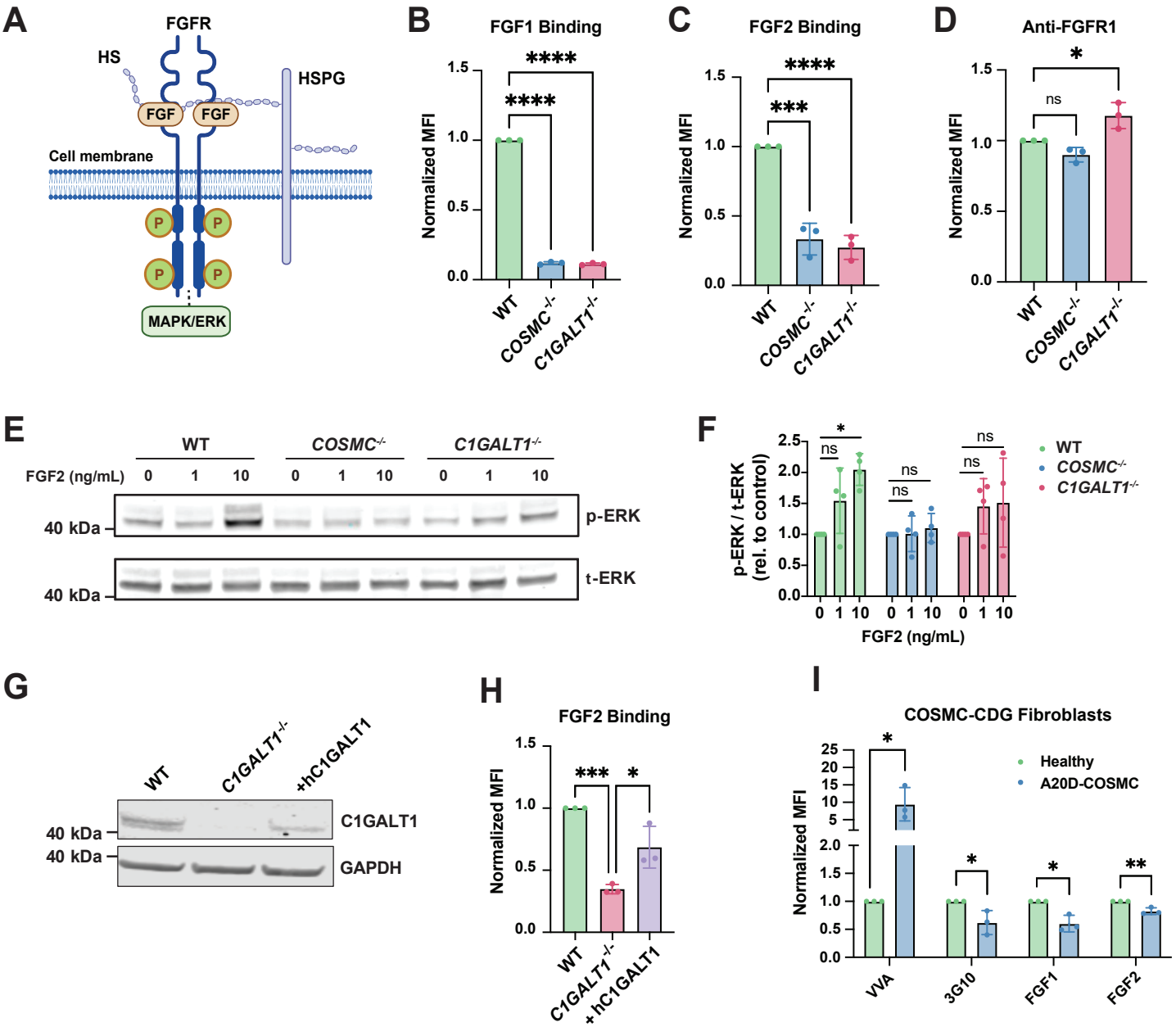
A
FGFR
HS
HSPG
FGF
FGF
Cell membrane
P
MAPK/ERK
B
FGF1 Binding
Normalized MFI
****
****
WT
COSMC-/-
C1GALT1-/-
C
FGF2 Binding
Normalized MFI
****
***
D
Anti-FGFR1
Normalized MFI
*
ns
E
WT
COSMC-/-
C1GALT1-/-
FGF2 (ng/mL)
0 1 10 0 1 10 0 1 10
40 kDa
p-ERK
t-ERK
F
p-ERK / t-ERK (rel. to control)
FGF2 (ng/mL)
WT
COSMC-/-
C1GALT1-/-
G
WT
C1GALT1-/-
+hC1GALT1
40 kDa
C1GALT1
GAPDH
H
FGF2 Binding
Normalized MFI
***
*
WT
C1GALT1-/-
+hC1GALT1
I
COSMC-CDG Fibroblasts
Healthy
A20D-COSMC
Normalized MFI
VVA
3G10
FGF1
FGF2

Figure 3

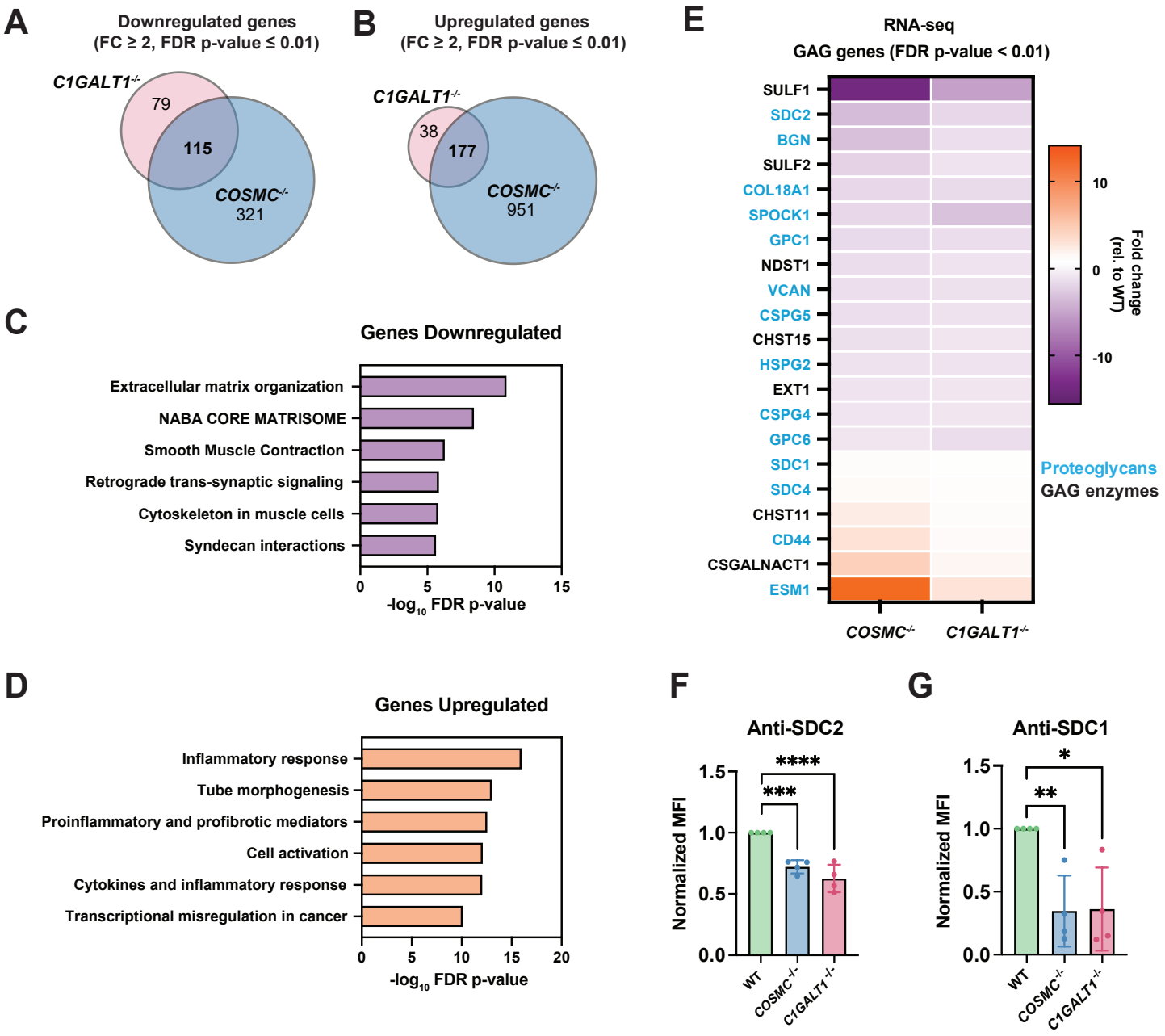
A
Downregulated genes
(FC ≥ 2, FDR p-value ≤ 0.01)
C1GALT1-/-
79
115
COSMC-/-
321
B
Upregulated genes
(FC ≥ 2, FDR p-value ≤ 0.01)
C1GALT1-/-
38
177
COSMC-/-
951
C
Genes Downregulated
Extracellular matrix organization
NABA CORE MATRISOME
Smooth Muscle Contraction
Retrograde trans-synaptic signaling
Cytoskeleton in muscle cells
Syndecan interactions
0
5
10
15
-log10 FDR p-value
D
Genes Upregulated
Inflammatory response
Tube morphogenesis
Proinflammatory and profibrotic mediators
Cell activation
Cytokines and inflammatory response
Transcriptional misregulation in cancer
0
5
10
15
20
-log10 FDR p-value
E
RNA-seq
GAG genes (FDR p-value < 0.01)
SULF1
SDC2
BGN
SULF2
COL18A1
SPOCK1
GPC1
NDST1
VCAN
CSPG5
CHST15
HSPG2
EXT1
CSPG4
GPC6
SDC1
SDC4
CHST11
CD44
CSGALNACT1
ESM1
COSMC-/-
C1GALT1-/-
10
0
-10
Fold change
(rel. to WT)
Proteoglycans
GAG enzymes
F
Anti-SDC2
Normalized MFI
1.5
1.0
0.5
0.0
****
***
WT
COSMC-/-
C1GALT1-/-
G
Anti-SDC1
Normalized MFI
1.5
1.0
0.5
0.0
*
**
WT
COSMC-/-
C1GALT1-/-

Figure 4

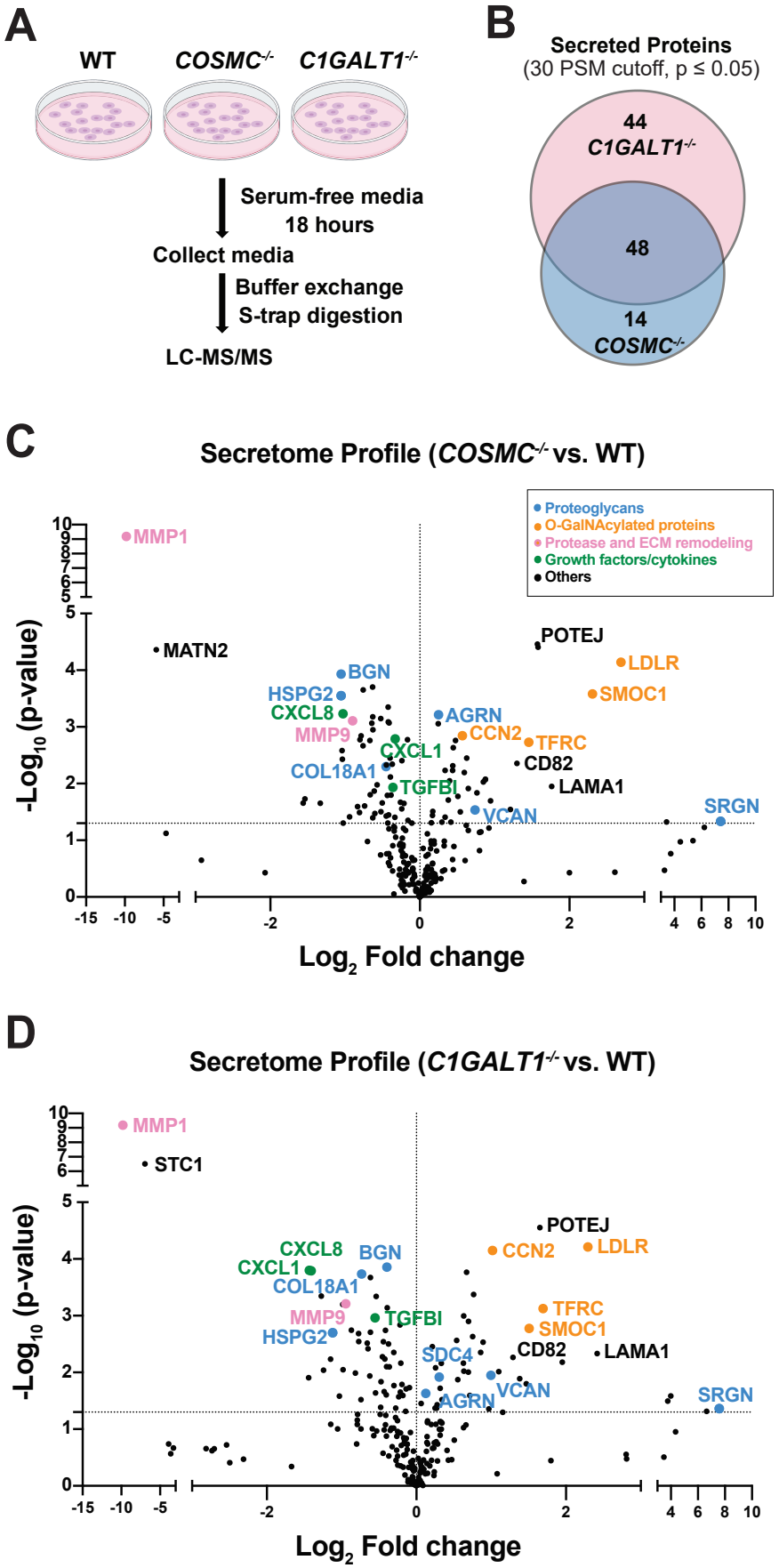
A
WT
COSMC-/-
C1GALT1-/-
Serum-free media
18 hours
Collect media
Buffer exchange
S-trap digestion
LC-MS/MS
B
Secreted Proteins
(30 PSM cutoff, p ≤ 0.05)
44
C1GALT1-/-
48
14
COSMC-/-
C
Secretome Profile (COSMC-/- vs. WT)
Proteoglycans
O-GalNAcylated proteins
Protease and ECM remodeling
Growth factors/cytokines
Others
MMP1
MATN2
POTEJ
LDLR
SMOC1
BGN
HSPG2
CXCL8
AGRN
MMP9
CCN2
TFRC
CXCL1
CD82
COL18A1
LAMA1
TGFBI
VCAN
SRGN
-Log10 (p-value)
Log2 Fold change
D
Secretome Profile (C1GALT1-/- vs. WT)
MMP1
STC1
POTEJ
CXCL8
BGN
CCN2
LDLR
CXCL1
COL18A1
TFRC
MMP9
TGFBI
SMOC1
HSPG2
SDC4
CD82
LAMA1
VCAN
AGRN
SRGN
-Log10 (p-value)
Log2 Fold change

Figure 5

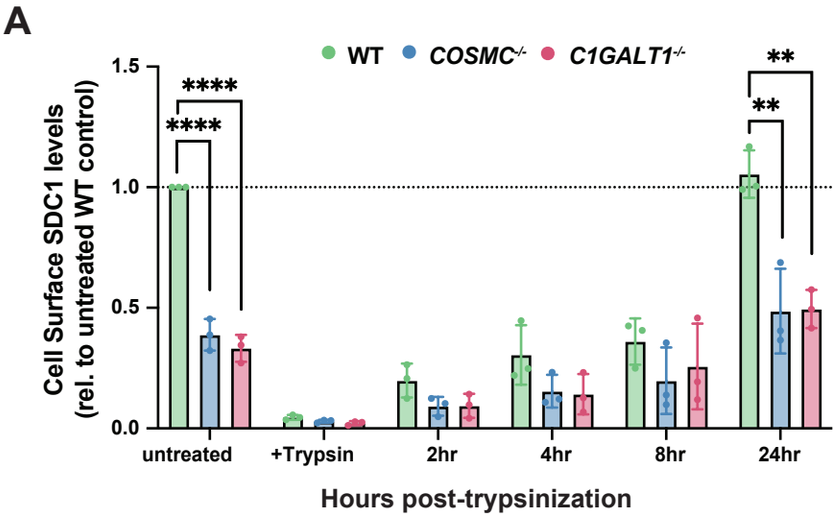

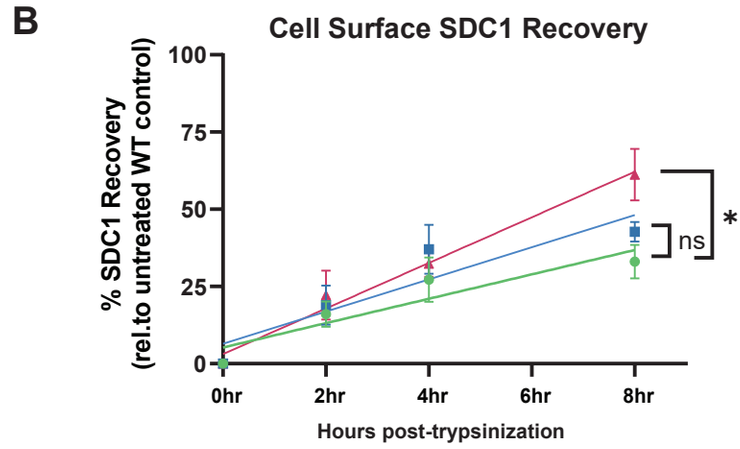

	WT	COSMC-/-	C1GALT1-/-
Slope	3.95 ± 0.90	5.2 ± 1.07	7.38 ± 0.97

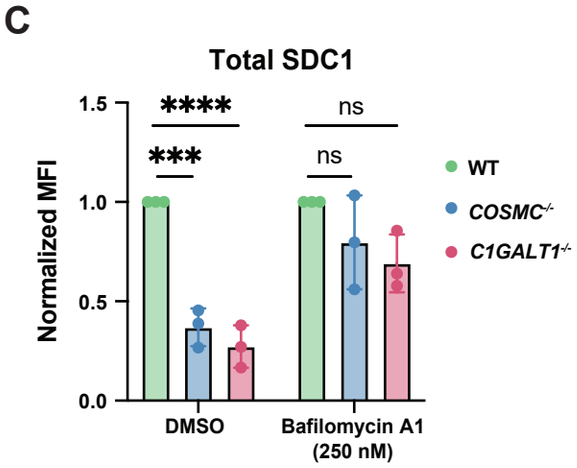

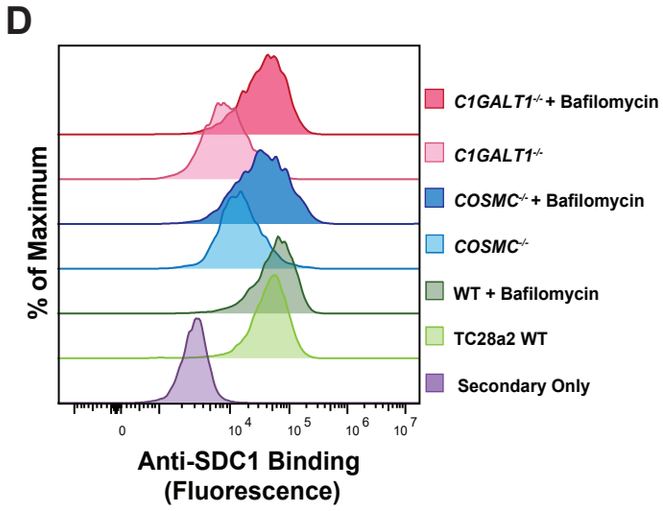

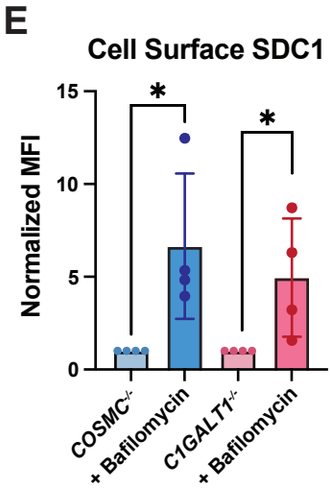

Figure 6

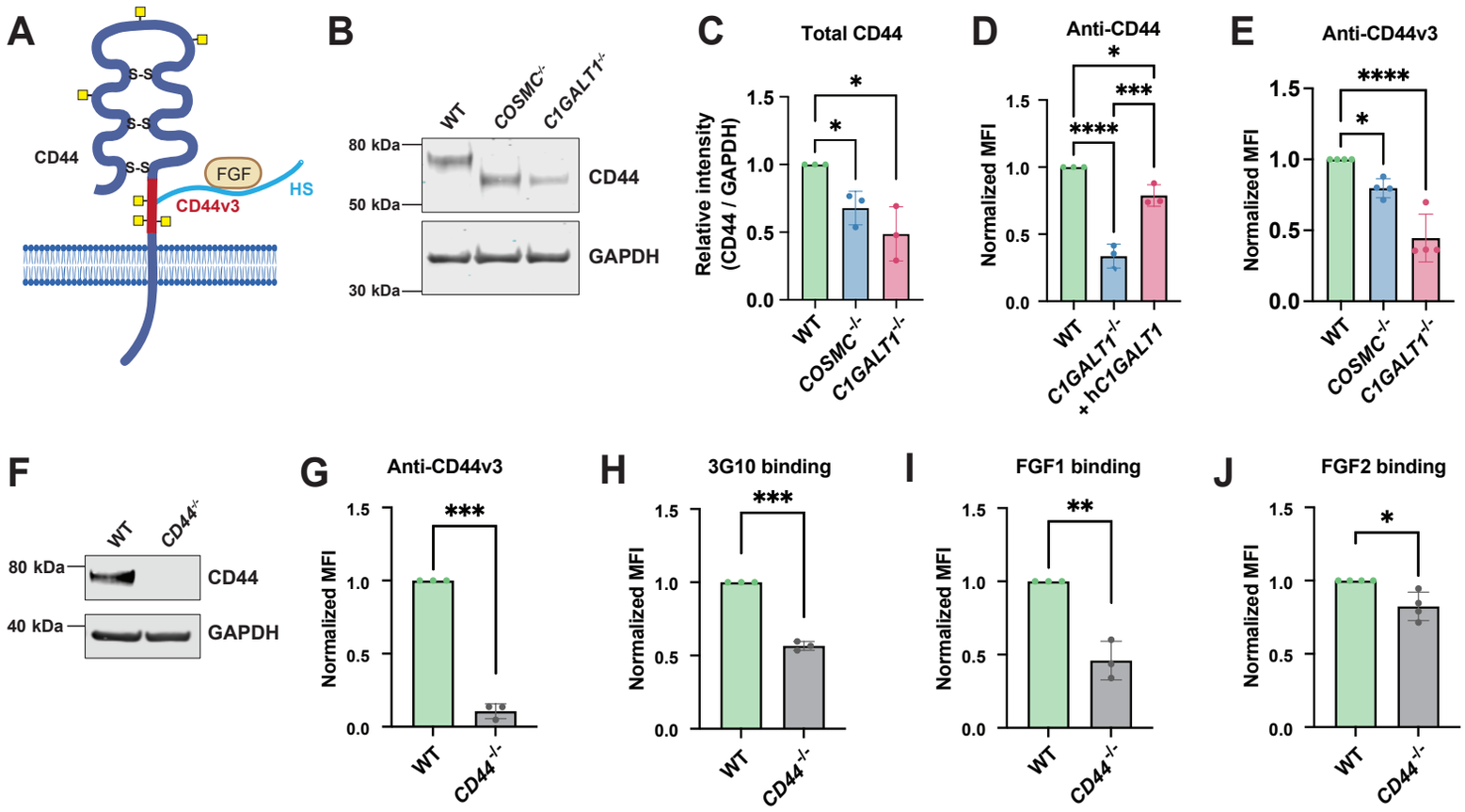
A
CD44
S-S
S-S
S-S
FGF
HS
CD44v3
B
WT
COSMC-/-
C1GALT1-/-
80 kDa
50 kDa
30 kDa
CD44
GAPDH
C
Total CD44
Relative intensity (CD44 / GAPDH)
1.5
1.0
0.5
0.0
*
*
WT
COSMC-/-
C1GALT1-/-
D
Anti-CD44
Normalized MFI
*
***
****
WT
C1GALT1-/-
C1GALT1-/- + hC1GALT1
E
Anti-CD44v3
Normalized MFI
****
*
WT
COSMC-/-
C1GALT1-/-

F
WT
CD44-/-
80 kDa
40 kDa
CD44
GAPDH
G
Anti-CD44v3
Normalized MFI
***
WT
CD44-/-
H
3G10 binding
Normalized MFI
***
WT
CD44-/-
I
FGF1 binding
Normalized MFI
**
WT
CD44-/-
J
FGF2 binding
Normalized MFI
*
WT
CD44-/-

Figure 7

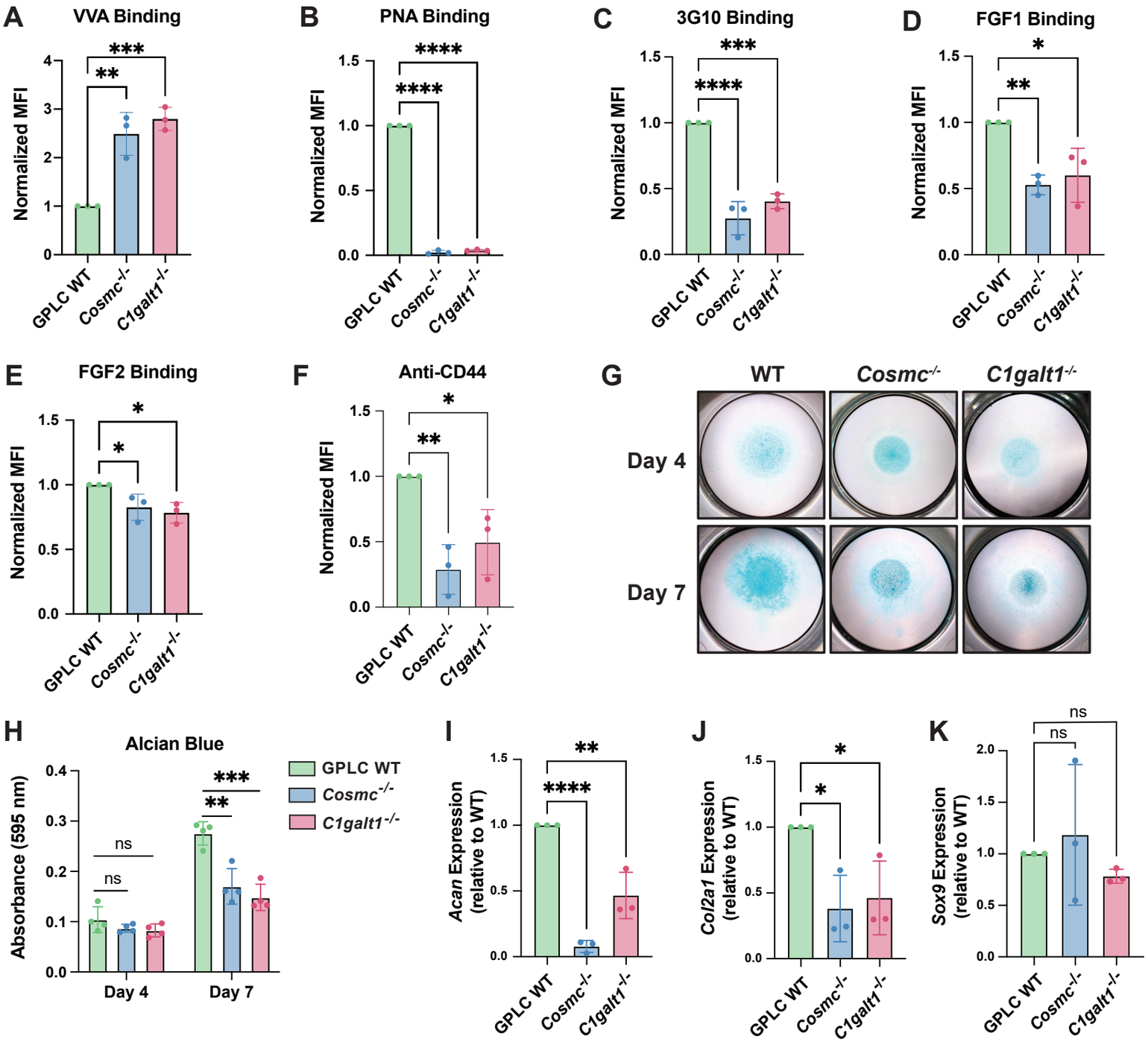
A
VVA Binding
Normalized MFI
0
1
2
3
4
**
***
GPLC WT
Cosmc-/-
C1galt1-/-
B
PNA Binding
Normalized MFI
0.0
0.5
1.0
1.5
****
****
GPLC WT
Cosmc-/-
C1galt1-/-
C
3G10 Binding
Normalized MFI
0.0
0.5
1.0
1.5
***
****
GPLC WT
Cosmc-/-
C1galt1-/-
D
FGF1 Binding
Normalized MFI
0.0
0.5
1.0
1.5
*
**
GPLC WT
Cosmc-/-
C1galt1-/-
E
FGF2 Binding
Normalized MFI
0.0
0.5
1.0
1.5
*
*
GPLC WT
Cosmc-/-
C1galt1-/-
F
Anti-CD44
Normalized MFI
0.0
0.5
1.0
1.5
*
**
GPLC WT
Cosmc-/-
C1galt1-/-
G
WT
Cosmc-/-
C1galt1-/-
Day 4
Day 7
H
Alcian Blue
Absorbance (595 nm)
0.0
0.1
0.2
0.3
0.4
ns
ns
**
***
Day 4
Day 7
GPLC WT
Cosmc-/-
C1galt1-/-
I
Acan Expression (relative to WT)
0.0
0.5
1.0
1.5
**
****
GPLC WT
Cosmc-/-
C1galt1-/-
J
Col2a1 Expression (relative to WT)
0.0
0.5
1.0
1.5
*
*
GPLC WT
Cosmc-/-
C1galt1-/-
K
Sox9 Expression (relative to WT)
0.0
0.5
1.0
1.5
2.0
ns
ns
GPLC WT
Cosmc-/-
C1galt1-/-

Figure 8

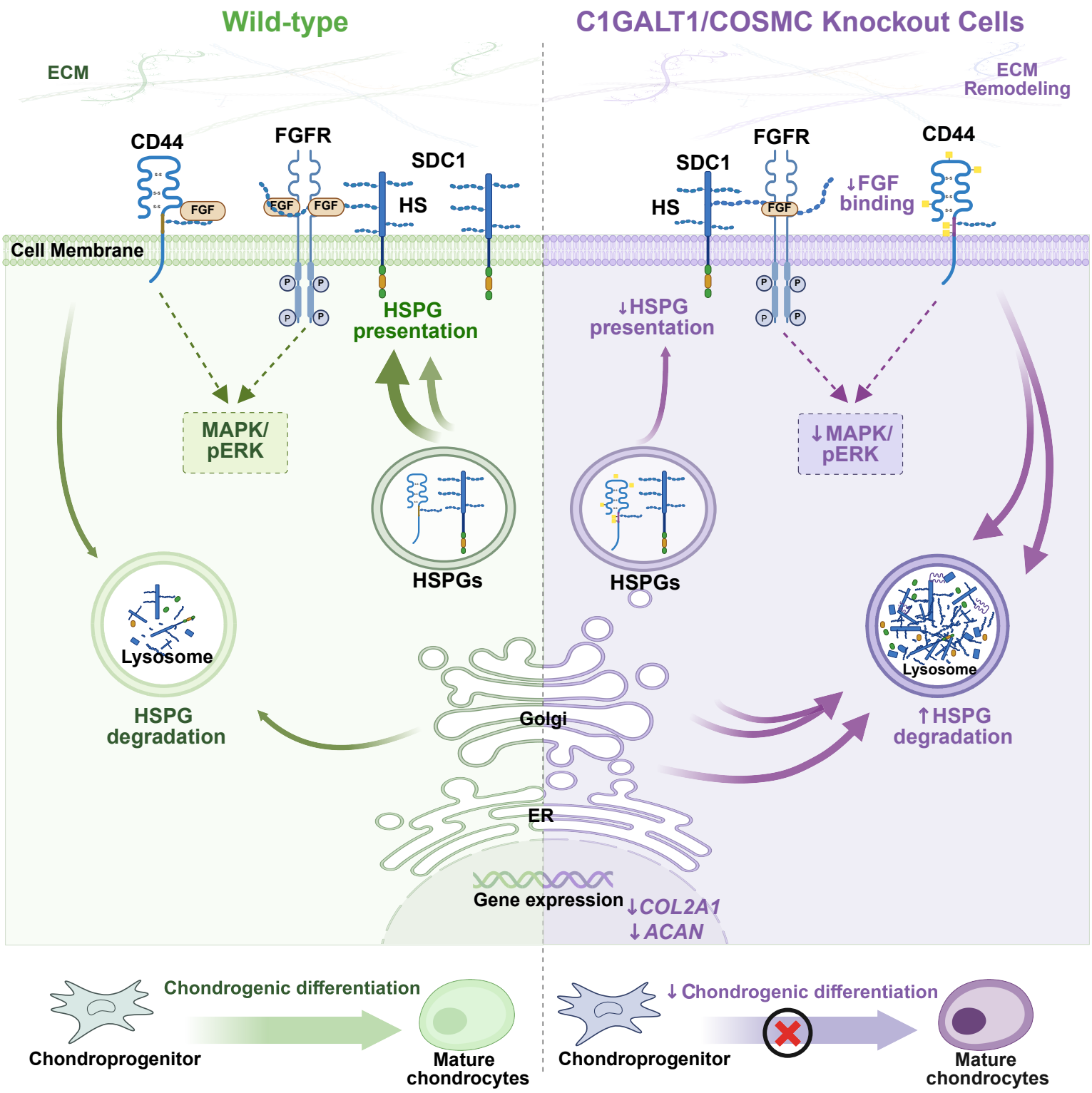
Wild-type
C1GALT1/COSMC Knockout Cells
ECM
ECM Remodeling
CD44
FGFR
SDC1
HS
FGF
Cell Membrane
HSPG presentation
MAPK/ pERK
HSPGs
Lysosome
HSPG degradation
↓HSPG presentation
↓FGF binding
↓MAPK/ pERK
↑HSPG degradation
Golgi
ER
Gene expression
↓COL2A1
↓ACAN
Chondrogenic differentiation
Chondroprogenitor
Mature chondrocytes
↓ Chondrogenic differentiation

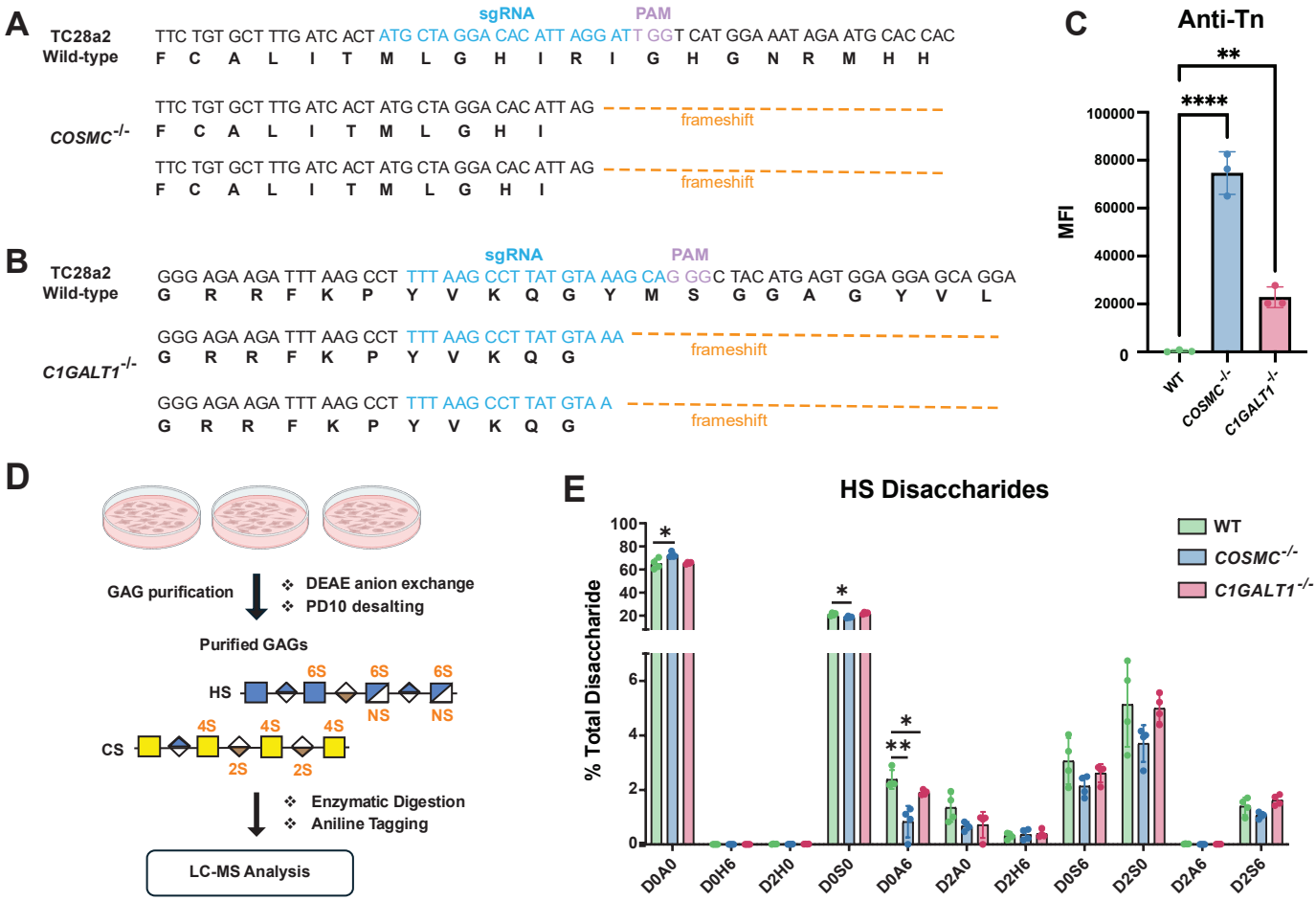
A
TC28a2 Wild-type
sgRNA
PAM
TTC TGT GCT TTG ATC ACT ATG CTA GGA CAC ATT AGG ATT GGT CAT GGA AAT AGA ATG CAC CAC
F C A L I T M L G H I R I G H G N R M H H
COSMC-/-
TTC TGT GCT TTG ATC ACT ATG CTA GGA CAC ATT AG
F C A L I T M L G H I
frameshift
TTC TGT GCT TTG ATC ACT ATG CTA GGA CAC ATT AG
F C A L I T M L G H I
frameshift
B
TC28a2 Wild-type
sgRNA
PAM
GGG AGA AGA TTT AAG CCT TTT AAG CCT TAT GTA AAG CAG GGC TAC ATG AGT GGA GGA GCA GGA
G R R F K P Y V K Q G Y M S G G A G Y V L
C1GALT1-/-
GGG AGA AGA TTT AAG CCT TTT AAG CCT TAT GTA AA
G R R F K P Y V K Q G
frameshift
GGG AGA AGA TTT AAG CCT TTT AAG CCT TAT GTA A
G R R F K P Y V K Q G
frameshift
C
Anti-Tn
MFI
WT
COSMC-/-
C1GALT1-/-
D
GAG purification
DEAE anion exchange
PD10 desalting
Purified GAGs
HS
CS
Enzymatic Digestion
Aniline Tagging
LC-MS Analysis
E
HS Disaccharides
% Total Disaccharide
WT
COSMC-/-
C1GALT1-/-
D0A0
D0H6
D2H0
D0S0
D0A6
D2A0
D2H6
D0S6
D2S0
D2A6
D2S6
F
HS Sulfates Per Disaccharide
% Total Disaccharide
Unsulfated
1-SO3
2-SO3
3-SO3
G
HS Sulfation
% Total Disaccharide
Unsulfated
N-SO3
2-O-SO3
6-O-SO3
H
CS Disaccharides
% Total Disaccharide
D0a0
D2a0
D0a6
D0a4
D2a6
D2a4
D0a10
I
CS Sulfation
% Total Disaccharide
Unsulfated
2-O-SO3
4-O-SO3
6-O-SO3

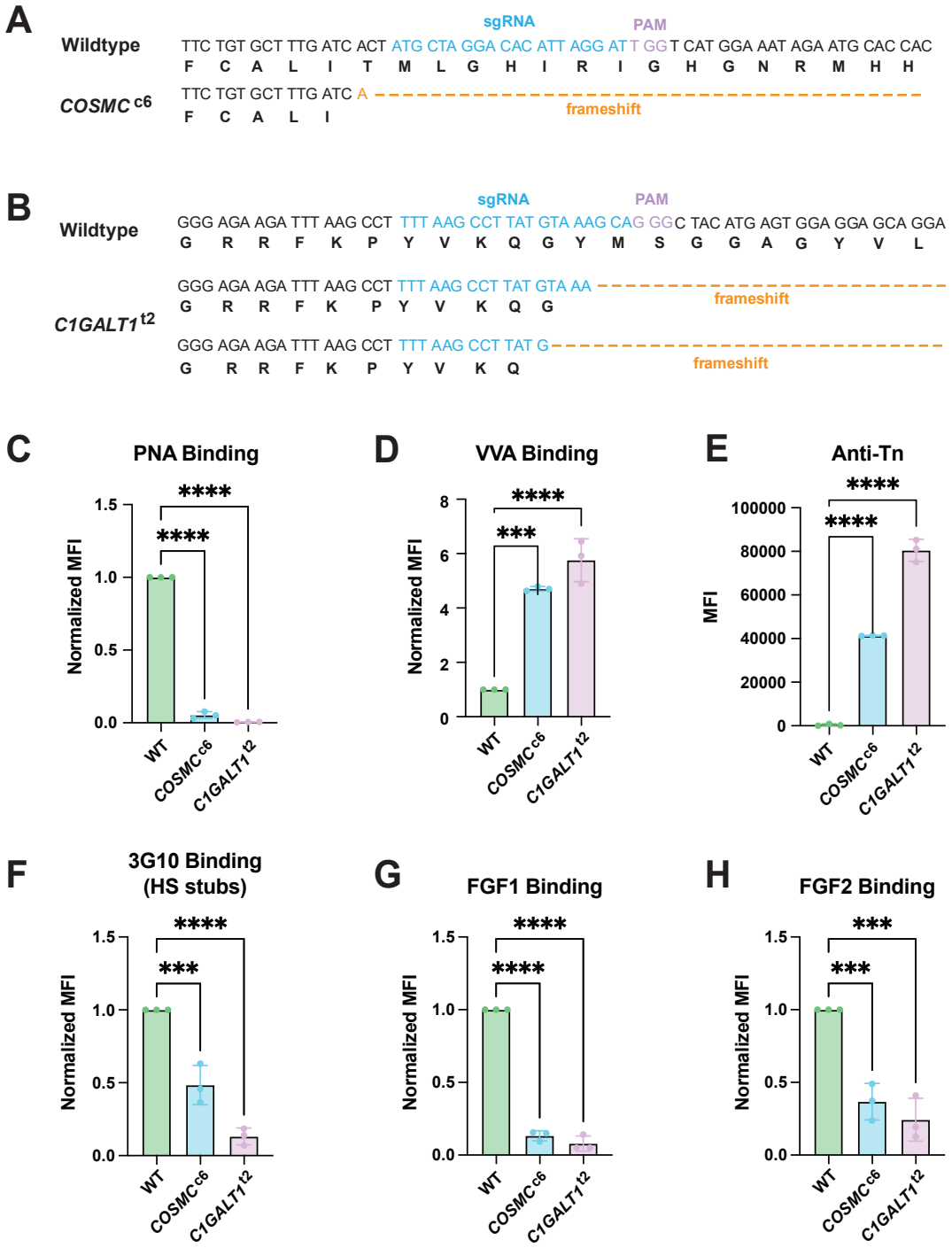
A
sgRNA
PAM
Wildtype
TTC TGT GCT TTG ATC ACT ATG CTA GGA CAC ATT AGG ATT GGT CAT GGA AAT AGA ATG CAC CAC
F C A L I T M L G H I R I G H G N R M H H
COSMC c6
TTC TGT GCT TTG ATC A
F C A L I
frameshift
B
sgRNA
PAM
Wildtype
GGG AGA AGA TTT AAG CCT TTT AAG CCT TAT GTA AAG CAG GGC TAC ATG AGT GGA GGA GCA GGA
G R R F K P Y V K Q G Y M S G G A G Y V L
C1GALT1 t2
GGG AGA AGA TTT AAG CCT TTT AAG CCT TAT GTA AA
G R R F K P Y V K Q G
frameshift
GGG AGA AGA TTT AAG CCT TTT AAG CCT TAT G
G R R F K P Y V K Q
frameshift
C
PNA Binding
Normalized MFI
****
****
WT
COSMC c6
C1GALT1 t2
D
VVA Binding
Normalized MFI
****
***
E
Anti-Tn
MFI
****
****
F
3G10 Binding
(HS stubs)
Normalized MFI
****
***
G
FGF1 Binding
Normalized MFI
****
****
H
FGF2 Binding
Normalized MFI
***
***

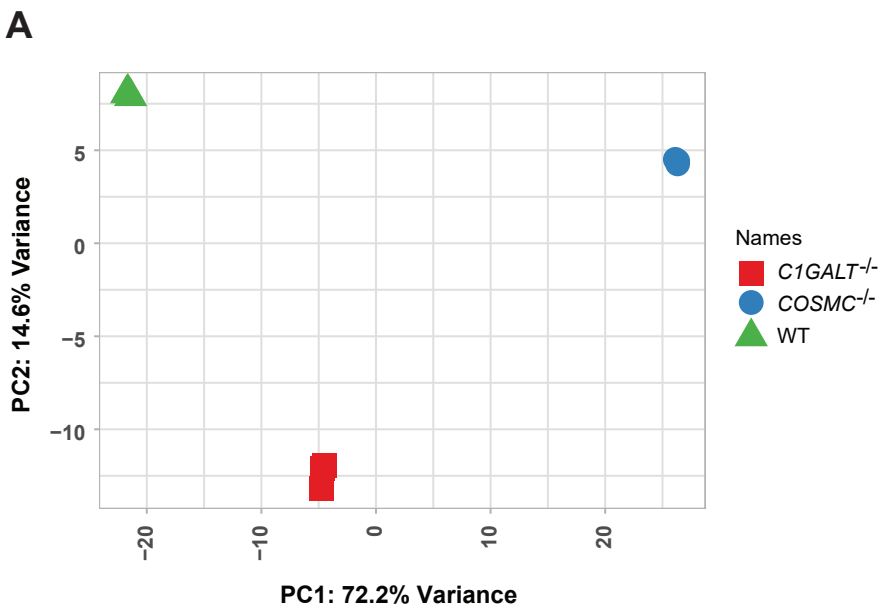
A
PC2: 14.6% Variance
PC1: 72.2% Variance
5
0
−5
−10
−20
−10
0
10
20
Names
C1GALT-/-
COSMC-/-
WT

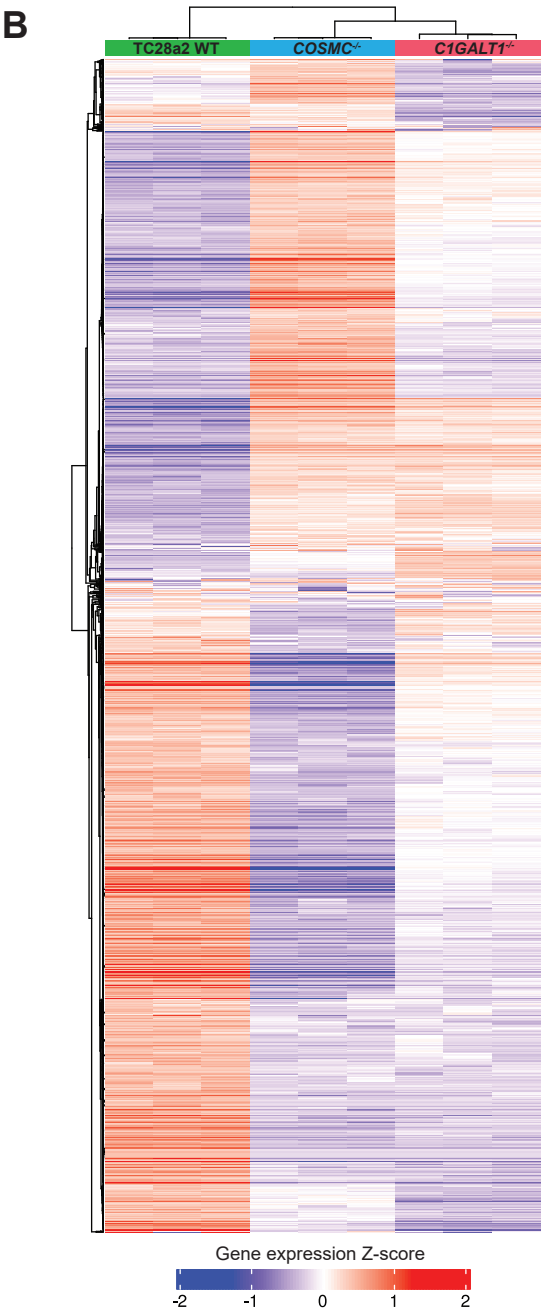
B
TC28a2 WT
COSMC-/-
C1GALT1-/-
Gene expression Z-score
-2
-1
0
1
2

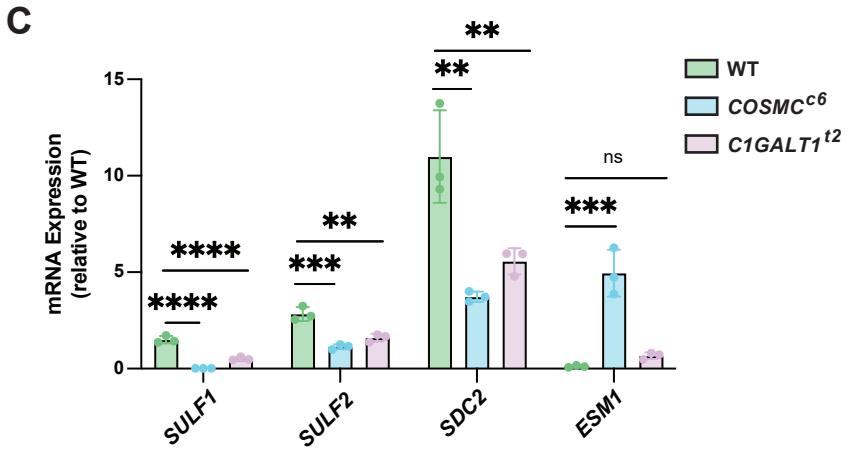
C
mRNA Expression (relative to WT)
15
10
5
0
****
****
***
**
**
**
***
ns
SULF1
SULF2
SDC2
ESM1
WT
COSMCc6
C1GALT1t2

Suppl Fig 4

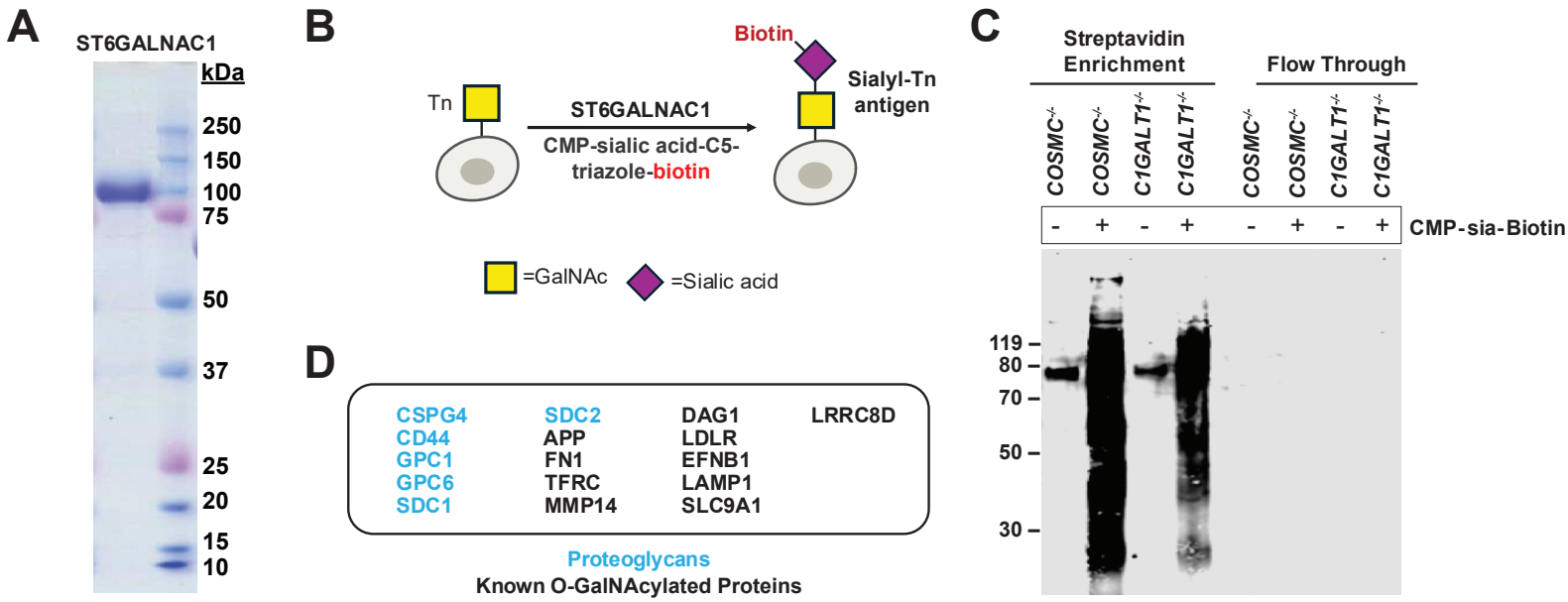
A
ST6GALNAC1
kDa
250
150
100
75
50
37
25
20
15
10
B
Tn
ST6GALNAC1
CMP-sialic acid-C5-triazole-biotin
Biotin
Sialyl-Tn antigen
=GalNAc
=Sialic acid
C
Streptavidin Enrichment
Flow Through
COSMC-/-
COSMC-/-
C1GALT1-/-
C1GALT1-/-
COSMC-/-
COSMC-/-
C1GALT1-/-
C1GALT1-/-
- + - + - + - +
CMP-sia-Biotin
119
80
70
50
30
D
CSPG4
CD44
GPC1
GPC6
SDC1
SDC2
APP
FN1
TFRC
MMP14
DAG1
LDLR
EFNB1
LAMP1
SLC9A1
LRRC8D
Proteoglycans
Known O-GalNAcylated Proteins

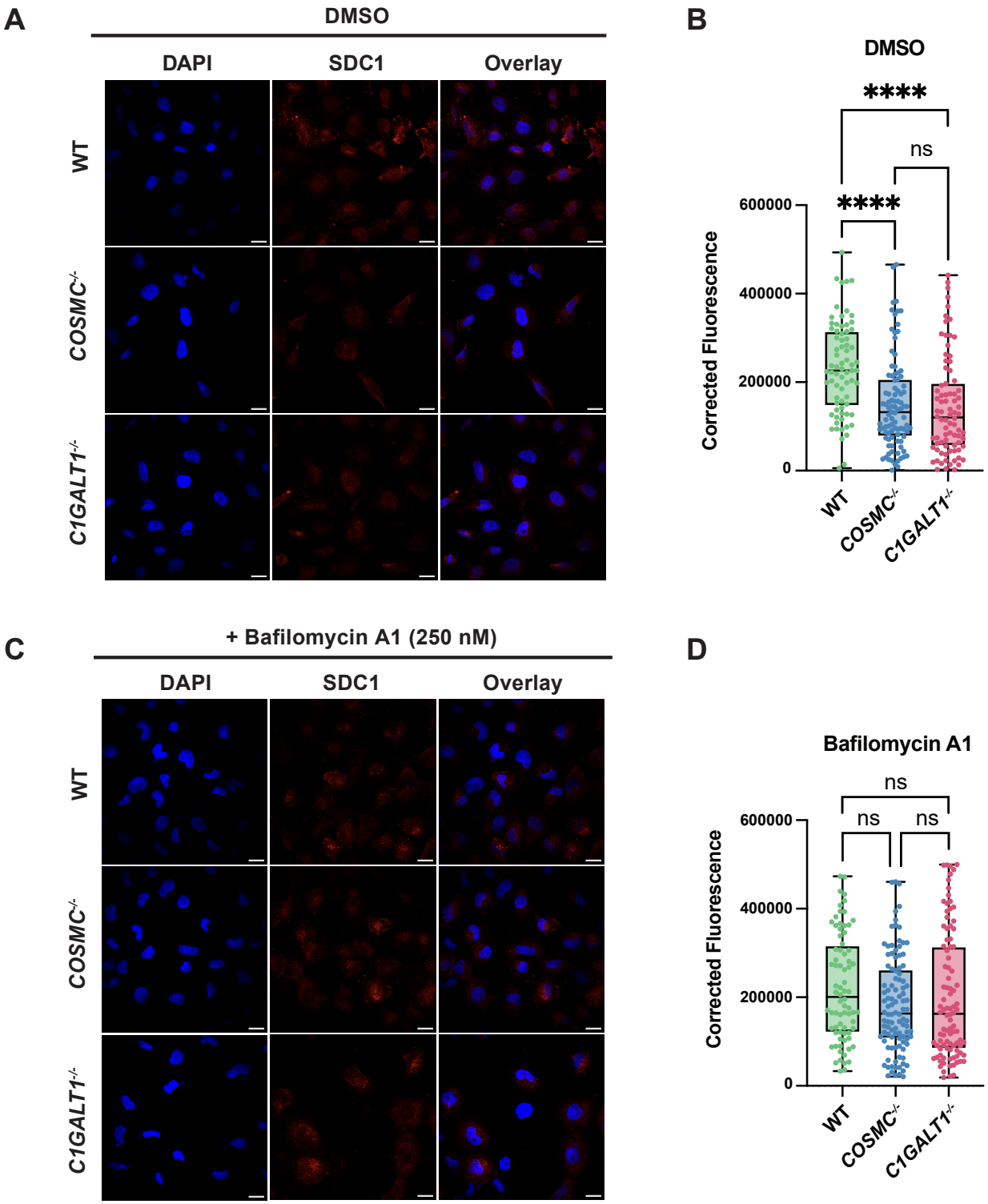
A
DMSO
DAPI
SDC1
Overlay
WT
COSMC-/-
C1GALT1-/-
B
DMSO
****
ns
****
600000
400000
200000
0
Corrected Fluorescence
WT
COSMC-/-
C1GALT1-/-
C
+ Bafilomycin A1 (250 nM)
DAPI
SDC1
Overlay
WT
COSMC-/-
C1GALT1-/-
D
Bafilomycin A1
ns
ns
ns
600000
400000
200000
0
Corrected Fluorescence
WT
COSMC-/-
C1GALT1-/-

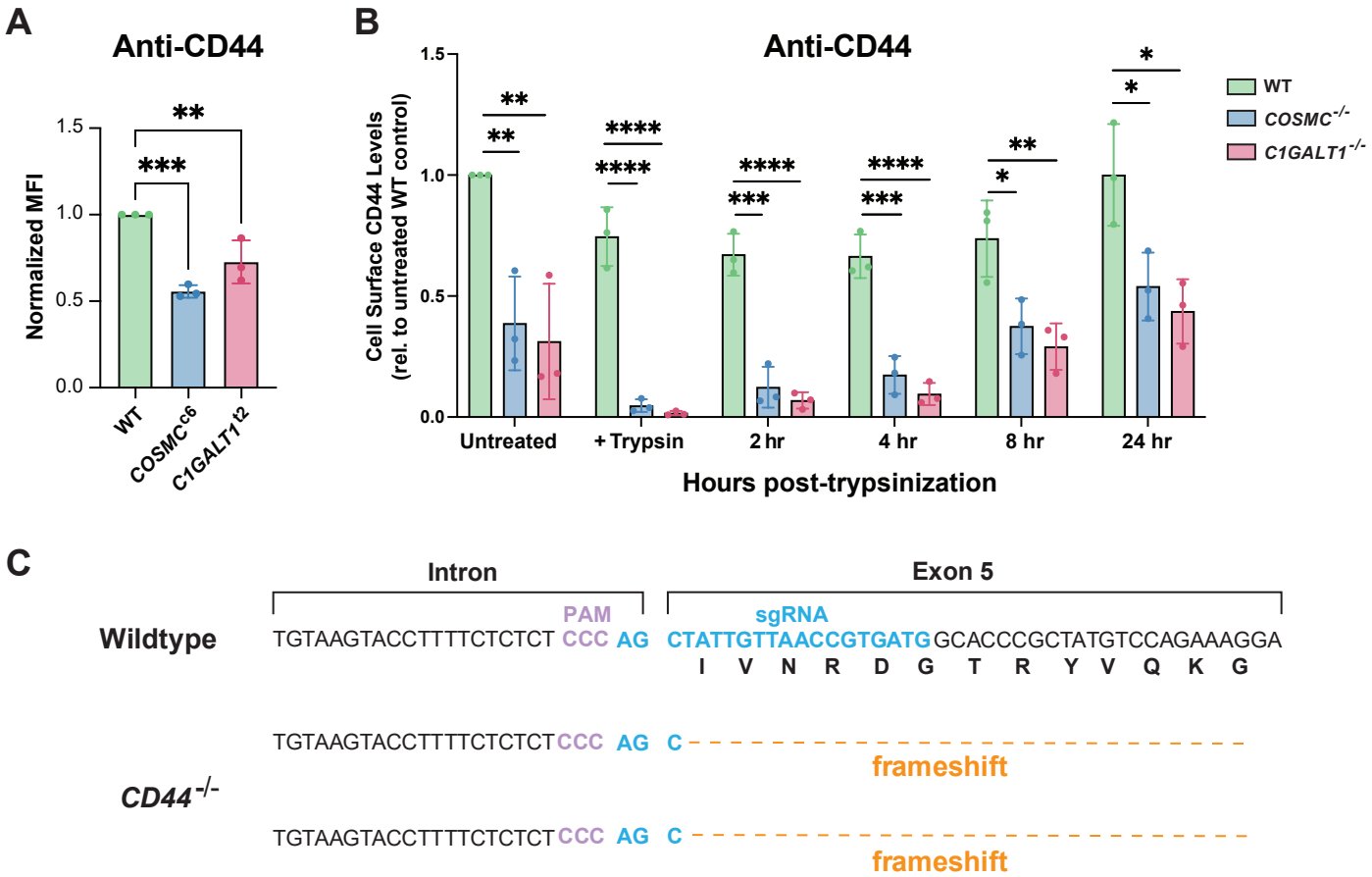
A
Anti-CD44
Normalized MFI
1.5
1.0
0.5
0.0
**
***
WT
COSMC c6
C1GALT1 t2
B
Anti-CD44
Cell Surface CD44 Levels
(rel. to untreated WT control)
1.5
1.0
0.5
0.0
**
**
****
****
****
***
****
***
**
*
*
*
Untreated
+ Trypsin
2 hr
4 hr
8 hr
24 hr
Hours post-trypsinization
WT
COSMC-/-
C1GALT1-/-
C
Intron
Exon 5
PAM
sgRNA
Wildtype
TGTAAGTACCTTTTCTCTCT CCC AG CTATTGTTAACCGTGATG GCACCCGCTATGTCCAGAAAGGA
I V N R D G T R Y V Q K G
TGTAAGTACCTTTTCTCTCT CCC AG C
frameshift
CD44-/-
TGTAAGTACCTTTTCTCTCT CCC AG C
frameshift

Suppl Fig 7

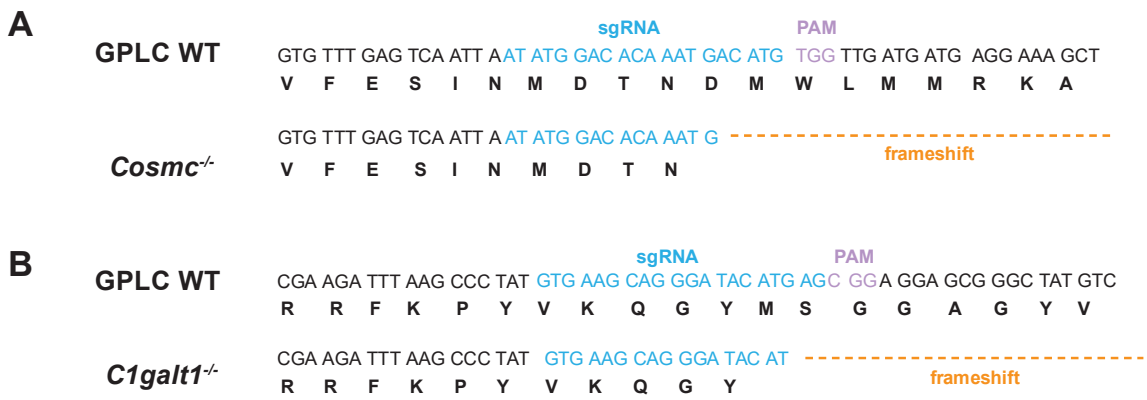
A
GPLC WT
sgRNA
PAM
GTG TTT GAG TCA ATT AAT ATG GAC ACA AAT GAC ATG TGG TTG ATG ATG AGG AAA GCT
V F E S I N M D T N D M W L M M R K A
Cosmc-/-
GTG TTT GAG TCA ATT A AT ATG GAC ACA AAT G
frameshift
V F E S I N M D T N
B
GPLC WT
sgRNA
PAM
CGA AGA TTT AAG CCC TAT GTG AAG CAG GGA TAC ATG AGC GGA GGA GCG GGC TAT GTC
R R F K P Y V K Q G Y M S G G A G Y V
C1galt1-/-
CGA AGA TTT AAG CCC TAT GTG AAG CAG GGA TAC AT
frameshift
R R F K P Y V K Q G Y